HIGH TEMPERATURE DEFORMATION AND FRACTURE OF Mg–0.5% Zr ALLOY

by

SAMBHULAL AGARWALA

DEPARTMENT OF METALLURGICAL ENGINEERING

INDIAN INSTITUTE OF TECHNOLOGY KANPUR

JANUARY, 1986

HIGH TEMPERATURE DEFORMATION AND FRACTURE OF Mg–0.5% Zr ALLOY

A Thesis Submitted
in Partial Fulfilment of the Requirements
for the Degree of

MASTER OF TECHNOLOGY

by

SAMBHULAL AGRARWALA

to the

DEPARTMENT OF METALLURGICAL ENGINEERING

INDIAN INSTITUTE OF TECHNOLOGY KANPUR

JANUARY, 1986

ME-1986-M-AGA-HIG

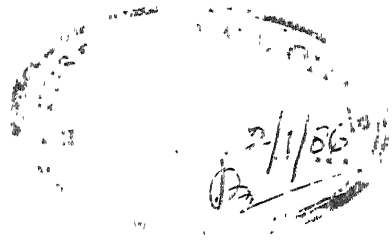

CERTIFICATE

This is to certify that the present investigation 'HIGH TEMPERATURE DEFORMATION AND FRACTURE OF Mg - 0.5% Zr ALLOY', has been carried out by Mr. Sambhu Lal Agarwala under my supervision and that it has not been submitted elsewhere for a degree.

(S. P. Gupta)
Assistant Professor
Department of Metallurgical Engineering
Indian Institute of Technology
Kanpur, India

ACKNOWLEDGEMENTS

I take this opportunity to express my sincere and profound gratitude to Professor G.S. Murty for introducing me to the area of superplasticity and extending enthusiastic aid throughout the present investigation. His continuous encouragement and innumerable stimulating discussions provided a pleasant academic environment that I am fond of remembering.

My thanks are also due to Dr. S.P. Gupta for valuable help and suggestions.

Sincere thanks are also due to friends Mr. R.S. Mishra and Mr. Alok Kanti Goswami for their cooperation during the work, and Mr. R.N. Srivastava for typing this report.

- Sambhu Lal Agarwala

TABLE OF CONTENTS

LIST OF TABLES

LIST OF FIGURES

ABSTRACT

High temperature deformation and fracture behaviour of the Mg - 0.5% Zr alloy has been studied in this investigation for specimens of grain sizes of 40 μm and 125 μm. The temperature range investigated for deformation was 0.68 to 0.95 T_m, where T_m is the melting point of the alloy in K. All the fracture tests were carried out at 648 K. The stress-strain rate behaviour has been studied by means of differential strain rate tests.

Two regions are observed in the $\sigma - \dot{\varepsilon}$ plots of steady state deformation at various temperatures. The flow behaviour is rate sensitive at lower strain rates (region II) even for this large grained material. Rate insensitive flow is observed at higher strain rates (region III). In the superplastic region II, the strain rate sensitivity index m is 0.5 ± 0.1 whereas grain size exponent is 1.9. The activation energy for deformation in region II is 67.3 KJ/mole which is close to the grain boundary self diffusion in magnesium. The experimental constitutive equations of region II are in better agreement with models of Ball and Hutchison, and Mukherjee for superplasticity.

In region III, the observed m, Q and p values are 0.20 ± 0.01, 116.4 KJ/mole and zero respectively. These observations in region III are consistent with the predictions of high temperature dislocation climb controlled creep.

Microstructural instability during deformation has also been investigated through repeated strain rate cycling. Specimens of grain size 40 μm from as received extruded bar do not show any mechanical instability/microstructural instability at relatively lower temperatures. However, microstructural coarsening occurs at very high temperatures. Specimens from as received rolled sheet having a grain size of 125 μm show microstructural instability even at intermediate temperature due to inhomogeneity in structure. This instability is reduced by giving annealing treatment to the specimens before testing.

In the fracture tests elongation to failure increases with decrease in strain rate i.e. with increase in strain rate sensitivity index and with decrease in grain size. Depending on the imposed strain rate, failure in the material occurs by quasistable plastic flow, necking or quasibrittle failure. Though considerable cavitation occurs at all strain rates final failure occurs by ductile tearing rather than 'cavitation'. This is because of the difficulty in the interlinkage of cavities during deformation.

CHAPTER I

INTRODUCTION

One of the earliest types of engineering centered around the extraction, forming and utilization of metals. The art and technology of metal forming was born with the ancients' discovery that heating metal pieces greatly improved malleability. However, the very ease of metal deformation at elevated temperatures presents the problem of maintaining dimensional limits in high temperature service applications, such as high pressure steam boilers, gas turbine engines, petrochemical refineries, etc. Over the years, metallurgists have tried to enhance resistance to the creep deformation by alloying or by incorporating at the microstructural level, stable, fine, and chemically inert dispersions. The results have often been dramatic.

In recent years another line of investigation, also at elevated temperatures, has opened up new and exciting possibilities to such studies. Instead of trying to restrict creep deformation, this new approach takes full advantage of the ease of formation at elevated temperatures; the metal or alloy can be made to deform to strains often in excess of 2000% without fracture. The extremely large ductility associated with such deformation is termed superplasticity.

Superplasticity is no longer a scientific curiosity nor it is just a topic of academic interest. The process is finding extensive application in viable metal forming

practices, such as manufacture of components of titanium, aluminium, copper, iron, nickel, zirconium and zinc alloys [1].

Therefore, it is not surprising that the considerable attention has been given to this particular mode of deformation in recent years which has resulted in major advances [1, 2] in our understanding of the process. Despite this progress several issues remain unclarified. This missing information represents a major deficiency in our current knowledge, and it also limits our ability to predict operative ranges in terms of stress, temperature, grain size, and strain rate for the manifestation of the superplastic deformation phenomenon.

1.1 Deformation Behaviour of Superplastic Materials

The experimental and empirical data for metals and alloys when deformed at temperatures above $0.4\ T_m$ (T_m = melting temperature in K) can be represented in the form of a single equation for steady state creep rate ($\dot{\varepsilon}$) [3-6]

$$\dot{\varepsilon} = \frac{AEb}{kT} \left(\frac{b}{d}\right)^p \left(\frac{\sigma}{E}\right)^n D_o \exp\left(-\frac{Q}{RT}\right) \qquad (1)$$

where σ is the stress, A dimensionless parameter, E the Young's modulus, b the Burger's vector, k the Boltzman constant, T the absolute temperature, d the grain size, D_o the frequency factor, Q the activation energy, R the gas constant, $n = \frac{\partial(\ln \dot{\varepsilon})}{\partial(\ln \sigma)}$ stress exponent and $p = \frac{\partial(\ln \dot{\varepsilon})}{\partial(\ln d)}$ is the grain size exponent.

Every high temperature diffusion controlled creep mechanism is completely and unequivocally determined by four

parameters in Equation (1) i.e. Q, A, n and p. In the literature on superplasticity, the stress exponent (n) is replaced by the strain rate sensitivity parameter, $m = \frac{\partial(\ln \sigma)}{\partial(\ln \dot{\varepsilon})} = \frac{1}{n}$. The strain rate sensitivity parameter describes the capacity of a material to resist necking and has been used as a criterion to assess proposed mechanisms of superplastic deformation.

Characterization of stress-strain rate behaviour is usually made by a differential strain rate test [7], in which strain rate is increased in successive steps and corresponding steady state flow stress is measured at constant temperature. At very low strain rates, steady state strain rates are measured over a range of applied stress in creep experiments at constant temperature. The data are plotted logarithmically as σ versus $\dot{\varepsilon}$, as shown in Figure 1.

The majority of reported data on superplasticity show a sigmoidal behaviour (Figure 1, Plot A) between the logarithms of stress and strain rate. This plot suggests that superplasticity (region II) is a transition region [8] from one mechanism operative at high strain rates (region III) to another at low strain rates (region I). However, the sigmoidal or S-shape of the plot is not universal and other shapes (Figure 1, Plots B, C and D) have also been reported. Figure 1, Plots B and D suggest that superplasticity is a unique mechanism in its own [9, 10], the range of strain rates where this mechanism is rate-controlling being limited by dislocation creep at high strain rates and by diffusional

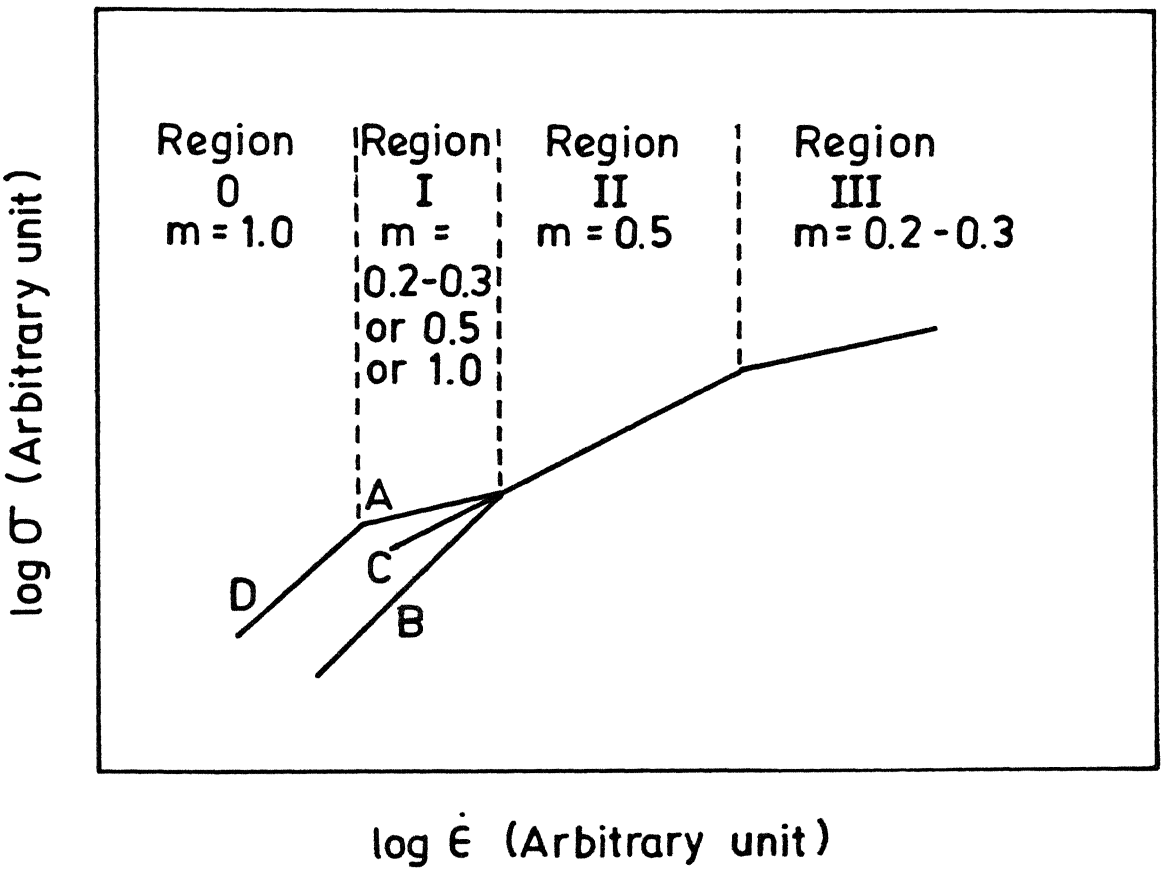

Fig. 1 Typical stress-strain rate plot (schematic)

creep at low strain rates. Moreover Figure 1, Plot D indicates that an additional deformation mechanism [11, 12] is rate controlling at strain rates that are intermediate between the strain rates for Region II and those for diffusional creep.

In region II, the strain rate sensitivity index, m, is significantly high, usually ≥ 0.5, leading to superplasticity. The ductility is maximum for highest m value and parameters like temperature and grain size have similar influence on both ductility and m. The decrease in grain size shifts region II to higher strain rates. Similarly, the increase in temperature of deformation reduces the overall level of the flow stress and displaces the region II to higher strain rates. The measured activation energies for deformation for region II generally fall into two categories: activation energies similar to those for grain boundary diffusion [11], and those comparable to the energy for lattice diffusion [13].

On the other hand, region III exhibits relatively rate insensitive flow behaviour, characteristic of the usual plastic flow. This region as mentioned earlier is generally attributed to some form of dislocation creep. The observations in region I are not consistent. These regions limit the superplastic range and thus have indirect importance.

1.2 Mechanism of Steady State Flow

It follows from equation (1) that the mechanism of flow in high temperature deformation is determined by the

activation energy, Q, the exponents n and p and to a lesser extent, the value of the dimensionless constant A. Several reviewers in recent times have summarized the various mechanisms of superplasticity [14-18]. Microscopic evidence indicate some intragranular dislocation activity in the superplastic region II, but the dominant deformation mechanism appears to be grain boundary sliding. The contribution from grain boundary sliding decreases at high (region III) and lower (region I) strain rates. Scratch mark experiments are generally used to estimate the contribution of grain boundary sliding to the total strain. The results of such studies are summarized in Table I. Although the results shown in the table were calculated by different procedures, which makes direct comparison difficult, the general trend, however, is the same in every investigation. Several mechanisms have been developed theoretically to explain the phenomenon of superplasticity but, without exception, each model is inconsistent with one or more of the established experimental trends [15]. The mechanisms of regions II and III are considered below.

1.2.1 Region II

The theories proposed for superplasticity are either rheological or atomistic. The atomistic theories can broadly be divided into

(a) Diffusional flow mechanisms,

(b) Dislocation creep theories, and

(c) Grain boundary deformation models.

Table I

Contribution of grain boundary sliding to the total axial strain $\varepsilon_{gb}/\varepsilon_t$ *

Material	$\varepsilon_{gb}/\varepsilon_t$ (%)		
	Region I	Region II	Region III
Zn - 22% Al	30	60	30
Pb - Tl		50	33
Mg - Al eutectic	12	64	29
Pb - Sn eutectic		70	
Pb - Sn eutectic	21	56	20
Mn - 1.5% Mn - 0.3% C	33	41 - 49	30
Al - 9% Zn - 1.0% Mg		63	26
Zn - 0.4% Al	42	48	28

* This table has been reproduced from Ref. [19].

1.2.1(a) Diffusional Flow Mechanisms

It is now well recognized that pure diffusional flow (N-H and Coble creep mechanisms) is inadequate in giving rise to large plastic strain in polycrystalline materials other than the bamboo-type grain structures. Ashby and Verrall [8] developed a theory based on grain boundary sliding with diffusional accommodation through the lattice as well as grain boundaries. The mechanism is derived from a grain switching event which leads to the retention of essentially equiaxed grain structure during superplastic deformation.

A group of four regular hexagonal grains in a two-dimensional model is considered. These grains through a neighbour-switching event move from the initial state to a final one with an identical grain shape. In this process, the grains undergo accommodation strains and translate past each other by grain boundary sliding. This gives a true strain of 0.55 as a result of this switching event. A constitutive equation based on this mechanism is derived and it is similar to the classical Nabarro-Herring-Coble equation but gives rise to a threshold stress for deformation and strain rates that are an order of magnitude faster. Because of the threshold stress, this mechanism predicts a sigmoidal relationship between stress and strain rate.

1.2.1(b) Dislocation Creep Theories

These theories are based on grain boundary sliding with accommodation by dislocation motion. According

to Ball and Hutchison [20], a group of grains slides as a unit along some common direction. A grain, which does not have its boundary along the common sliding direction and is across the sliding path of the group, acts as an obstacle to the sliding process. This leads to stress concentration resulting in emission of dislocations from triple points of the blocking grain and the dislocations move to the opposite boundary until the back stress prevents further activation of the source and sliding stops. The leading dislocation in the pile up then climbs into and along the grain boundary. This results in further sliding at a rate governed by the kinetics of dislocation climb along grain boundaries to annihilation sites. Mukherjee [21, 22] also developed a similar theory but the dislocations are assumed to emanate from ledges in the sliding boundary and the specific requirement of the movement of groups of grains is not necessary.

1.2.1(c) Grain Boundary Deformation Model

These models essentially have core-mantle approach. The roles of grain boundary sliding and other creep mechanisms are coupled to develop these models based on the division of grains into their central "cores" and peripheral "mantles". Grain boundary sliding and its accommodation are limited to the mantle. According to Gifkins [23], the σ^2 term could arise from grain boundary dislocations piled up against a triple point. Gittus [24, 25] has combined elements of other theories [8, 23] with the suggestion that super dislocations must move in interphase boundaries to maintain

alloy phase structure. Padmanabhan's theory [26] is derived from Ke's model [27] in which plastic flow occurs by the shearing of groups of atoms in the boundary plane, so that there is interchange of atoms and vacancies leading to a liquid like Newtonion viscous flow.

The parameters of the constitutive equations based on various mechanisms relevant to superplastic flow (region II) are summarized in Table II.

1.2.2 Region III Mechanisms

High temperature dislocation climb controlled creep [28] is believed to be the dominating process in region III. Typical values that represent such a mechanism are n = 4 to 5 and Q is the lattice diffusion activation energy. Such a mechanism predicts flow behaviour that is independent of grain size. But due to some grain size dependency of creep behaviour in fine grained materials, some empirical relation has been developed by Barrett, Lytton and Sherby [29] in order to account for this behaviour. A theoretical treatment has also been given by Gifkins [30] incorporating the grain size effect. In this model, the total creep rate is considered to be the cumulative effect of climb controlled creep, grain boundary sliding and its accommodation by the formation of triple point folds.

Table II

Parameters of the constitutive equations based on different mechanisms for region II

Mechanism	n	p	Q	A*
Nabarro-Herring diffusional flow	1	2	Q_l	13
Coble diffusional flow	1	3	Q_{gb}	48
Ball and Hutchison [20]	2	2	Q_{gb}	100
Mukherjee [21, 22]	2	2	Q_{gb}	75-150
Ashby and Verrall [8]	Limiting value of 1	2-3	$Q_{gb} - Q_l$	70
Gifkins [23]	Limiting value of 1	2	Q_{gb}	64
Gittus [24, 25]	Limiting value of 2	2	Q_{IPB}	53.4
Padmanabhan [26]	Limiting value of 1	2	Q_{gb}	-

* Values of A in equation (1) with shear modulus G in place of Young's modulus E.

1.3 Non-steady State Flow and Microstructural Instability

The various proposed mechanisms deal with the steady state deformation where the flow stress is a unique function of steady state strain rate, temperature and grain size. This implies that the strain parameter does not have any effect on the stress-strain rate behaviour. In other words, the steady state nature of deformation and the applicability of the proposed mechanisms are valid to the extent that the structure remains stable, beyond which the microstructural instability and the accompanying strain effects can become significant enough to invalidate the steady state mechanisms. If the stress-strain rate data of fine grained materials are being obtained by differential strain rate test [7], the above aspects are to be examined carefully in order to assess whether the data obtained would represent steady state or not. Significant difference [31] in the values of the strain rate sensitivity index obtained from the same data of the differential strain rate test is an example of the non-validity of steady state approximation. In some of the reported studies, there have been significant microstructural instabilities along with the accompanying effects, as reviewed by Surey and Baudelet [32]. These microstructural changes are briefly considered below.

The fine grains subjected to deformation at elevated temperature are likely to suffer from grain coarsening. Experimental indication is that there are large variations in the size of the grains or phases with strain, strain rate

and with temperature. For example, within one cycle of differential strain rate test, where the specimen elongation was no more than 30%, the fine equiaxed grains of Pb-Sn eutectic increased in size by a factor of 2.35 at 170°C [33]. In another study [34] superplastic deformation of as rolled Zn - 0.4% Al alloy has been reported to exhibit an increase in grain size by a factor of 8. This grain coarsening leads to an increase in stress level and decrease in m value. These microstructural changes can influence the $\sigma - \dot{\varepsilon}$ behaviour to some extent.

1.4 Fracture Behaviour of Superplastic Materials

Most metals exhibit only rather small strains to failure when pulled in tension, and the maximum possible ductility is generally less than 100%. By contrast superplastic metals are capable of very high tensile elongations under optimum conditions, so that failure often occurs after the material has pulled out to some hundreds, or even a few thousands, of per cent. As a result of this behaviour it was generally considered in early experiments that cavity formation was not important in superplastic deformation, and attention was directed primarily towards the development of macroscopic necking. However, more recent work has firmly established the importance of internal cavitation in many (if not most) superplastic alloys, and it is now recognized that the growth and interlinkage of cavities is an important parameter in controlling the ease and type of fracture.

Elongation to failure in superplasticity depends critically on the imposed strain rate, the testing temperature and the initial grain size. High elongations to failure are usually observed at intermediate strain rates and there is a decrease at both higher and lower rates of strain. Such large elongations to failure are associated with high m-values. A schematic plot of both elongation to failure and m-value versus strain rate is shown in Figure 2.

1.4.1 Types of Fracture in Superplastic Materials

At the macroscopic level there are four distinct and identifiable types of fracture in superplastic materials.

1.4.1(a) Failure by Quasi Stable Plastic Flow

True superplastic deformation requires that the material pulls out in tension to a fine wire in a manner directly analogous to the drawing of a glass rod in a flame to form a sender filament.

A stability condition may be established to designate the limit of uniform flow in tension by noting that, in general, the stress σ is related to the strain ε and strain rate $\dot{\varepsilon}$ by an equation of the form

$$\sigma = B \varepsilon^{N} \dot{\varepsilon}^{m} \qquad (2)$$

where N is the strain hardening exponent and B is a constant. Using equation (2) it may be shown that deformation is stable under the following condition [35]

$$(N/\varepsilon) + m \geq 1 \qquad (3)$$

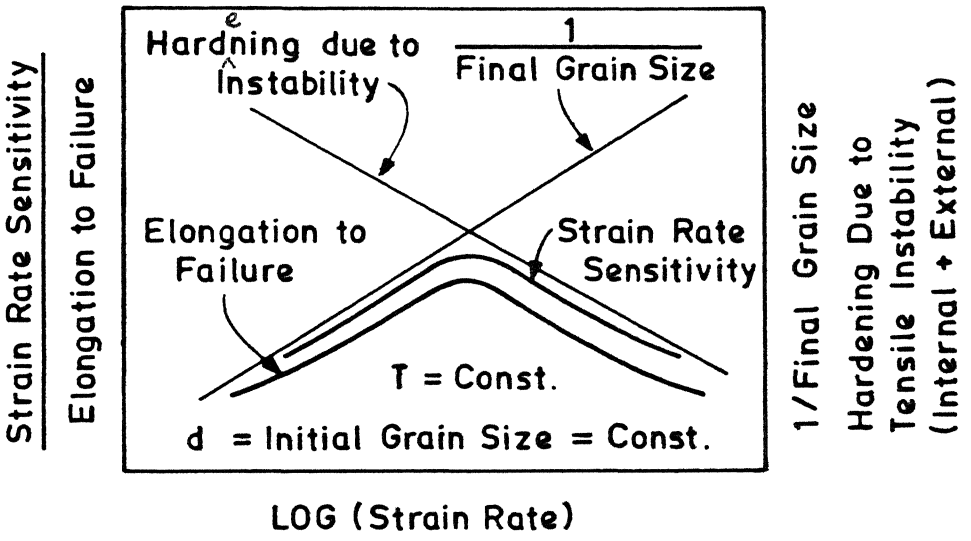

Fig. 2 Schematic representation of the elongation to failure dependence on strain rate.

In superplastic metals tested at relatively high temperatures, N is essentially zero and m is usually close to 0.5. Thus it is apparent that the stability criterion given by equation (3) is not satisfied. However, by combining equation (2) when N = 0 with the definitions of stress

$$\sigma = P/A \tag{4}$$

where P is the tensile force and A is the cross-sectional area, and strain rate at constant volume

$$\dot{\varepsilon} = -\left(\frac{1}{A}\right)\left(\frac{dA}{dt}\right) \tag{5}$$

where t is the time, it follows that

$$\frac{dA}{dt} = -\left(\frac{P}{B}\right)^{1/m} A^{(m-1)/m} \tag{6}$$

According to equation (6), the probability of necking decreases as $m \to 1$, and high value of m, typically ≥ 0.4, leads to diffuse necking and high elongations to failure.

Since m is usually of the order of 0.5, it is clear that, although true superplastic deformation as defined by an infinite elongation to failure is not a physically realistic process in a polycrystalline metal, a condition of optimal superplasticity is reasonably approximated when failure occurs by quasistable plastic flow in this condition the material pulls out to a fine point, so that

$$A_f/A_i \to 0$$

where A_f is the final fracture area where failure takes place and A_i the initial cross-sectional area within the

gauge length. The equivalent elongation at the failure point ε_A is given by

$$\varepsilon_A(\%) = \left(\frac{A_i}{A_f} - 1\right) \times 100 \qquad (7.)$$

so that $\varepsilon_A \to \infty$, with higher experimental values of ε_A occurring when m is increased.

1.4.1(b) Failure by Necking

Situations may arise in superplastic materials in which a sharp or localized neck develops and leads to catastrophic failure. Fracture by necking is termed as intrinsic plastic failure [36]. Intrinsic plastic failure is determined by the plastomechanical behaviour or constitutive equations of flow. A perturbation or incipient neck will not grow when the rate of hardening, $d\sigma_F/d\varepsilon$, is greater than the flow stress σ_F. Since σ_F is a function of many variables, including strain, strain rate, temperature, surface energy (γ), and various microstructural parameters, it is common to write

$$\frac{d\sigma_F}{d\varepsilon} = \frac{\partial\sigma_F}{\partial\varepsilon} + \frac{\partial\sigma_F}{\partial\dot{\varepsilon}}\left(\frac{d\dot{\varepsilon}}{d\varepsilon}\right) + \frac{\partial\sigma_F}{\partial T}\left(\frac{dT}{d\varepsilon}\right) + \frac{\partial\sigma_F}{\partial\gamma}\left(\frac{d\gamma}{d\varepsilon}\right) + \ldots \qquad (8)$$

Thus, the neck resistance of materials may derive from changes in any of these terms, either separately or in combination.

1.4.1(c) Cavitation Failure

As noted earlier, the formation of internal cavities is often important in superplastic materials and may

lead to cavitation failure in which fracture takes place in an abrupt manner with
little or no visible necking within the gauge length. Cavitation during superplasticity was first studied in Cu alloys but is now firmly established in a wide range of materials [37-42]. Observations show that cavities form early in the life of a specimen, and they are spread reasonably uniformly throughout the gauge length. The maximum level of cavitation in some materials corresponds to maximum ductility [43] whereas in other materials cavitation increases at the lower strain rates or is independent of strain rate. Since interfacial sliding is of major importance in the superplastic region II and thereby gives rise to cavitation, it is initially surprising that very high ductilities can be obtained. The answer lies in the mechanism of void growth and linkage whereby the instantaneous strain-rate sensitivity, and the strain-rate sensitivity of the work-hardening behaviour, affect the material properties on a microscopic scale, so that the tiny ligaments between cavities are themselves resistant to internal necking and micro-intrinsic plastic failure.

1.4.1(d) Quasibrittle Failure

Quasibrittle failure is a relatively unimportant fracture mode in superplastic materials; it tends to occur at low temperatures and at very high strain rates at the upper range of region III.

The characteristics of this mode of failure [44] are a high value of A_f/A_i ($\sim$0.6-0.8) so that $\varepsilon_A \simeq$ 25-75% and a low macroscopic elongation (typically, $\Delta L/L_o$ < 100%).

1.5 Objective of the Present Study

Most of the investigations in superplastic behaviour have been done on materials having grain sizes less than 10 μm. Very little work [47, 48] has been reported on 'superplasticity' in large grained materials. The present work has been taken up in order to explore the phenomenology in Mg - 0.5% Zr two phase alloy having grain size as large as 125 μm.

The stress-strain rate behaviour has been studied through the differential strain rate test. The parameters of the constitutive equation governing the steady state deformation have been determined experimentally in order to assess the operative mechanisms in regions II and III. Since the stability of microstructure is important for steady state deformation, extent of microstructural instability has also been studied. Finally to assess the fracture behaviour of the material elongation to failure at different initial strain rate has been determined and mode of fracture has also been studied.

CHAPTER II

EXPERIMENTAL PROCEDURE

In the present investigation Magnox ZR55A (from U.K.) magnesium base alloy was used. The alloy was obtained in the form of sheet with thickness 1.7 mm and extruded rod with diameter 12 mm. The chemical composition of this alloy is:

Constituent	Al	Zr	Fe	Si	Cu
wt pct	<0.020	>0.45 <0.65	<0.006	<0.01	<20 ppm

Ni	Zn	Mn	Ca	Mg
<10 ppm	<0.015	<0.010	<0.008	Bal.

2.1 Mechanical Testing

All the tests were done on an Instron 1195 testing machine. The tests were performed in tension making use of round and flat samples. True stress (σ), true strain (ε) and true strain rate ($\dot{\varepsilon}$) were calculated from the load-time record during deformation assuming uniform deformation along the gauge length. Special care was taken in maintaining precision of the load measurement in view of the small loads involved especially for flow at high test temperatures and low strain rates.

Typical dimensions of flat and round tensile samples are given in Figure 3. In case of fracture tests, samples with different dimension were used. Tensile samples were machined along the length of bars in case of round specimens

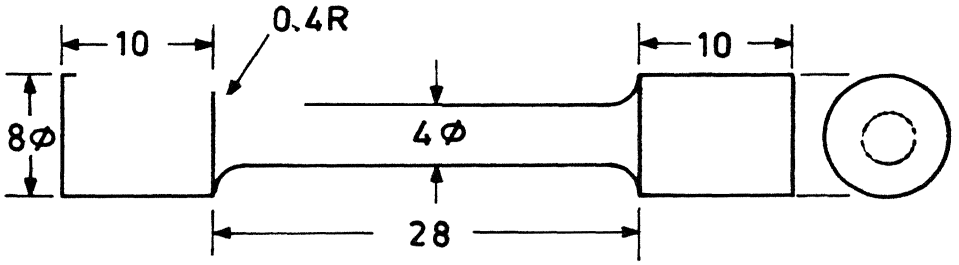

(a)

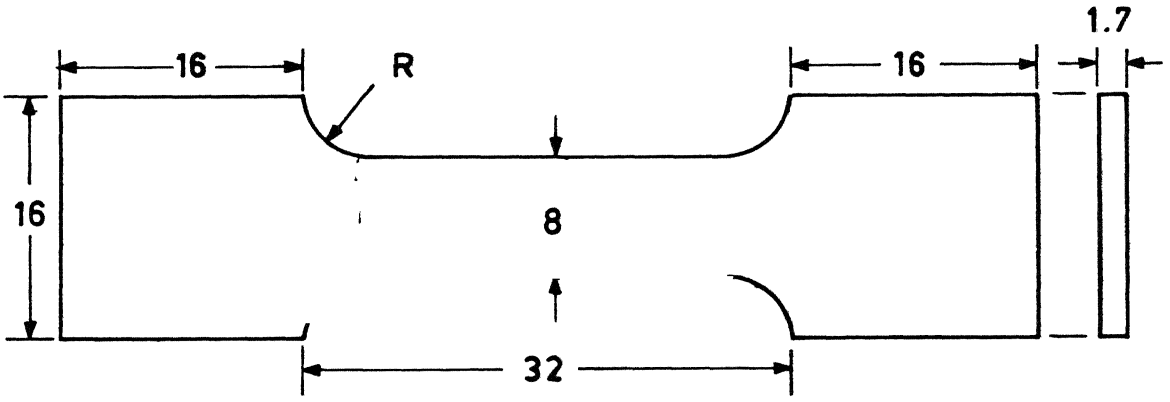

(b)

Dimensions are in mm

Fig. 3 Tensile test specimens (a) Round (b) Flat

and along the rolling direction in case of flat specimens.

Tensile tests were carried out at temperatures from 573 K to 873 K. The temperature was obtained using a three-zone vertical furnace and an on-off type temperature controller. A continuous monitor of the specimen temperature during each test showed that the variation in temperature was less than ± 1 K of the selected value.

2.1.1 Differential Strain-Rate Test

Differential strain rate method [7] was adopted to obtain stress-strain rate data of different specimens at various temperatures. Starting with the lowest cross head speed of 0.005 mm/min, the speed was successively increased to the next higher level to cover to a maximum speed of 2 mm/min. The load corresponding to each of the cross head speeds was thus recorded, from which, the true stress versus true strain rate data were calculated. In order to minimize the strain effects, the total strain accumulated in one cycle covering the whole range of cross head speeds was kept to a minimum level.

The strain rate sensitivity index 'm' was calculated either from the slope of $\log \sigma - \log \dot{\varepsilon}$ plot or in some cases from the relation

$$m = \frac{\log P_2/P_1}{\log V_2/V_1} \qquad (9)$$

where P_1 and P_2 are steady state loads corresponding to cross head speeds of V_1 and V_2 respectively.

Differential strain rate tests were conducted mostly in an incremental manner. In a few instances decremental tests were also carried out. The term "strain rate cycling" has the following connotation in the present work. The $\sigma - \dot{\varepsilon}$ data were collected by deforming a specimen between first and last strain rates to be investigated and this is defined as the first cycle. After this deformation the same specimen was further deformed over the same strain rate range thus giving a new value of stress for each of the strain rates, and this time $\sigma - \dot{\varepsilon}$ data are referred as the second-cycle data. This has been extended for more than two cycles in some cases.

2.1.2 Fracture Tests

All the fracture tests were conducted at 648 K at a number of cross head speeds. In order to maintain constant temperature throughout the length of the specimen small gauge length specimens were used. The dimensions for flat samples are: gauge length 12 mm and gauge width 6 mm. However, specimen dimension for the round samples were the same as those used in differential strain rate tests.

2.2 Metallography

For optical microscopy the surface of the samples was polished conventionally using series of emery papers, followed by cloth polishing with suspension of fine alumina powder. The etchants used was 15% HNO_3 in ethylene glycol.

The grain size measurement was done by using the linear-intercept method. The intercept length was converted to grain size by multiplying with a factor of 1.7/5.

For transmission electron microscopy Boltzmann technique was used for thinning the samples. The electrolyte used was 30% HNO_3 in methanol at a temperature of 4°C. For fractography study the fracture surfaces were observed in scanning electron microscope operating in secondary electron mode at 30 KV.

CHAPTER III

RESULTS

Experimental results are divided into three broad aspects of high temperature deformation and fracture. These are: Stress-strain rate behaviour, microstructural instability during deformation and fracture behaviour.

3.1 Deformation Behaviour

3.1.1 Microstructure and Stress-Strain Rate Behaviour

The grain size of the as received round samples and annealed (at 673 K for 12 hrs) flat samples were determined to be 40 μm and 125 μm respectively. Second phase particles were too small to be resolved optically. In order to determine the presence of second phase transmission electron microscopy was adopted. Figure 4 shows the electron micrograph and the SAD pattern of a sample of as received Mg - 0.5% Zr alloy. Precipitates were too small to be identified individually by SAD and added by the difficulty that Mg and α-Zr have very similar lattice parameters. The SAD pattern was therefore taken in an area containing precipitates. This resulted in a spotty ring pattern of α-Zr superimposed on Mg pattern (Figure 4(b)).

The $\sigma-\dot{\varepsilon}$ data for flat and round specimens at various temperatures are shown in Figures 5 and 6 respectively.

(a)

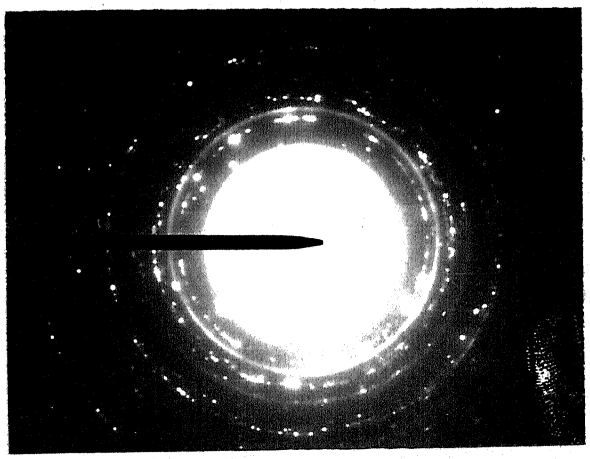

(b)

Fig. 4. Transmission electron micrographs from Mg - 0.5% Zr (a) as received, Magnification: X22,000, (b) SAD pattern of (a).

Figure 7 shows the $\sigma - \dot{\varepsilon}$ data for specimens of both the grain sizes at temperature of 648 K.

The observed $\sigma - \dot{\varepsilon}$ behaviour of specimens of both the grain sizes can be characterized as regions II and III of the high temperature steady state deformation. No region I was noticed in the investigated ranges of grain size, temperature and strain rate. The transition strain rate between regions II and III is observed to increase with increase in the test temperature for both the grain sizes and also with decreasing grain size at the test temperature of 648 K. The strain rate sensitivity index in each of the regions II and III is not significantly influenced by test temperature or grain size. In region II this value is 0.50 ± 0.10 whereas in region III it is 2.0 ± 0.01. As typical cases m versus $\dot{\varepsilon}$ plot at different temperatures is shown in Figure 8 for grain size of 125 μm.

3.1.2 Determination of Parameters of the Constitutive Equations

The experimental data have been analyzed in terms of typical steady state creep equation with the incorporation of grain size effect (equation 1). From the $\sigma - \dot{\varepsilon}$ data of regions II and III the grain size exponent (p), activation energy (Q) and the dimensionless constant (A) have been evaluated for each of the regions. As already mentioned, the variation of strain rate sensitivity index was within a narrow range for each of the regions and thus 'm' can be approximated as independent of grain size and temperature.

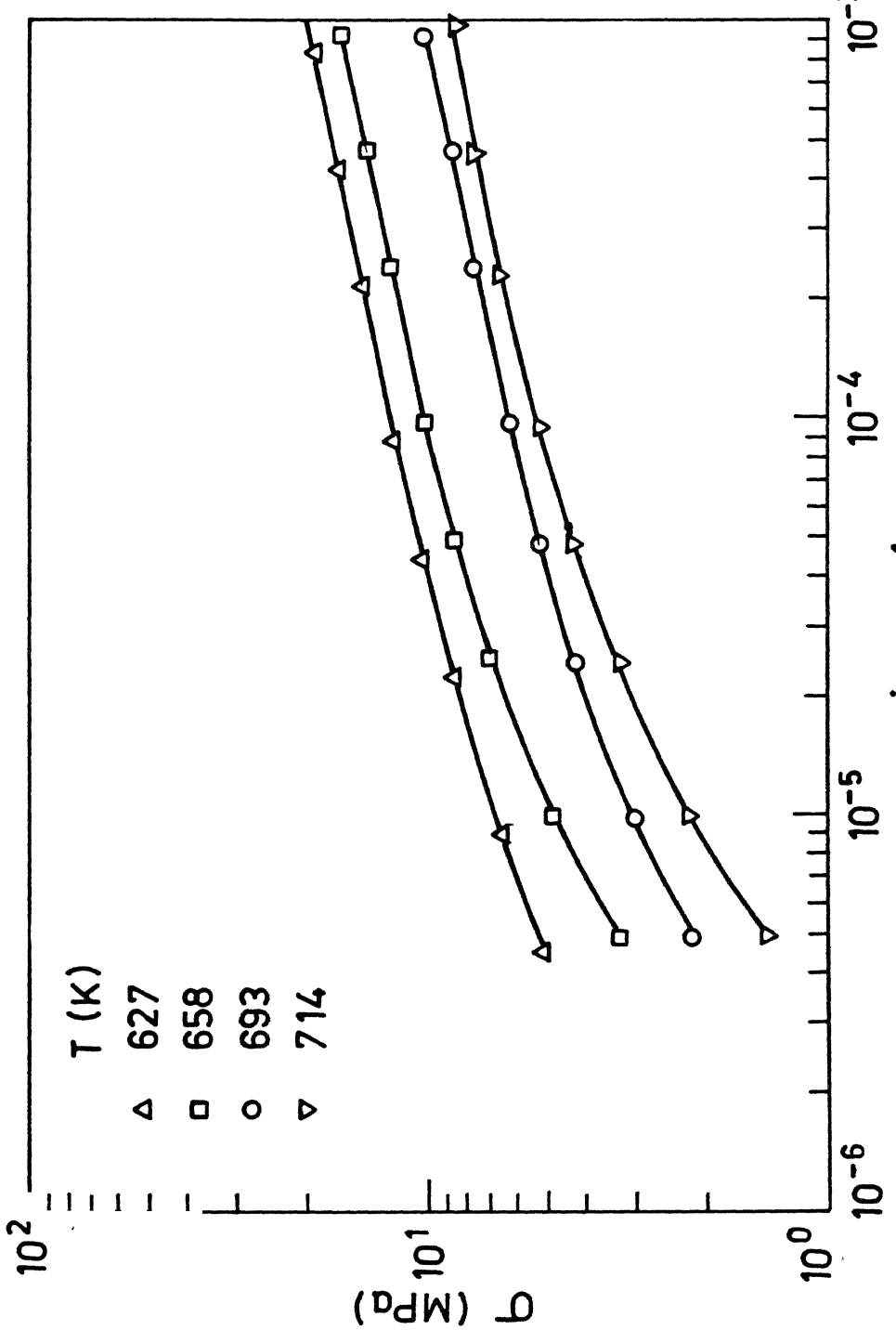

Fig. 5 Stress-strain rate plots for different temperatures (d = 125 μm)

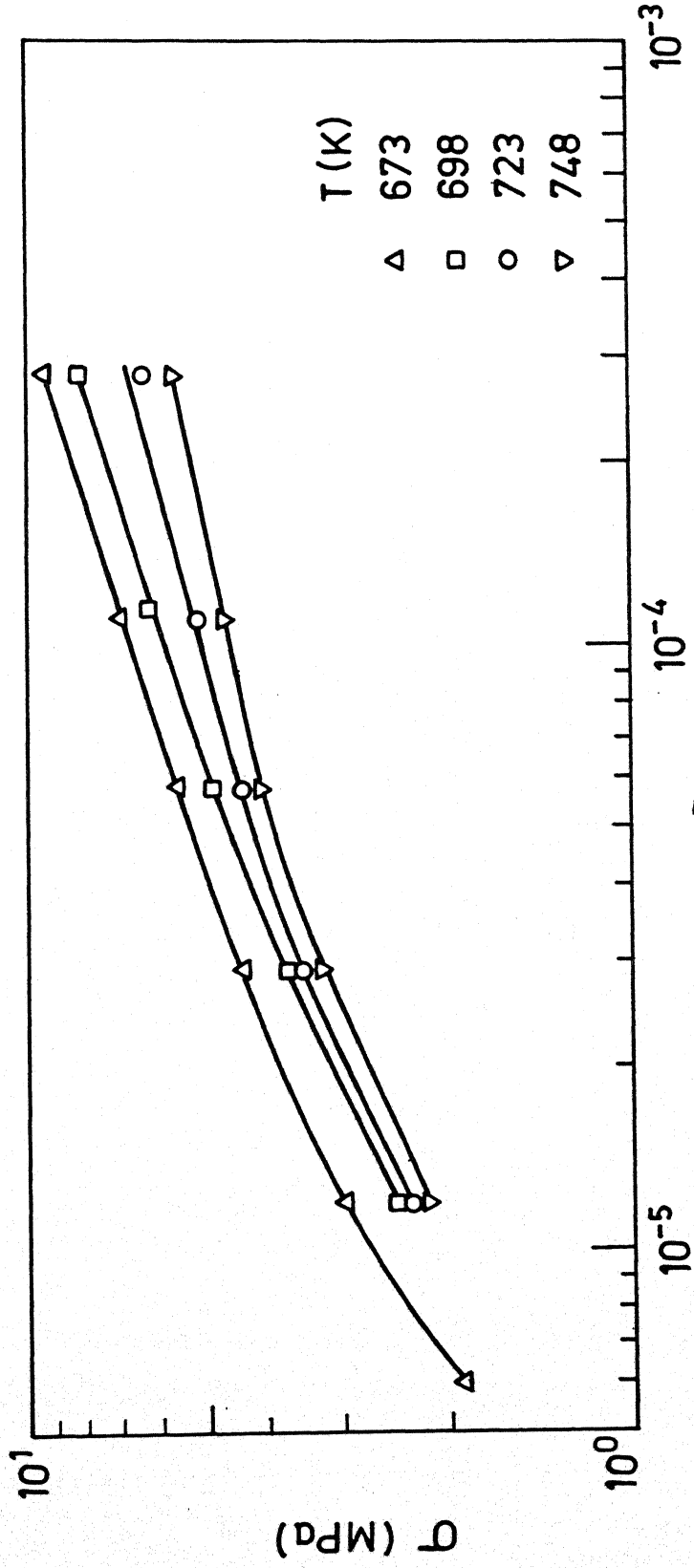

Fig. 6 Stress-strain rate plots for different temperatures (d = 40 μm)

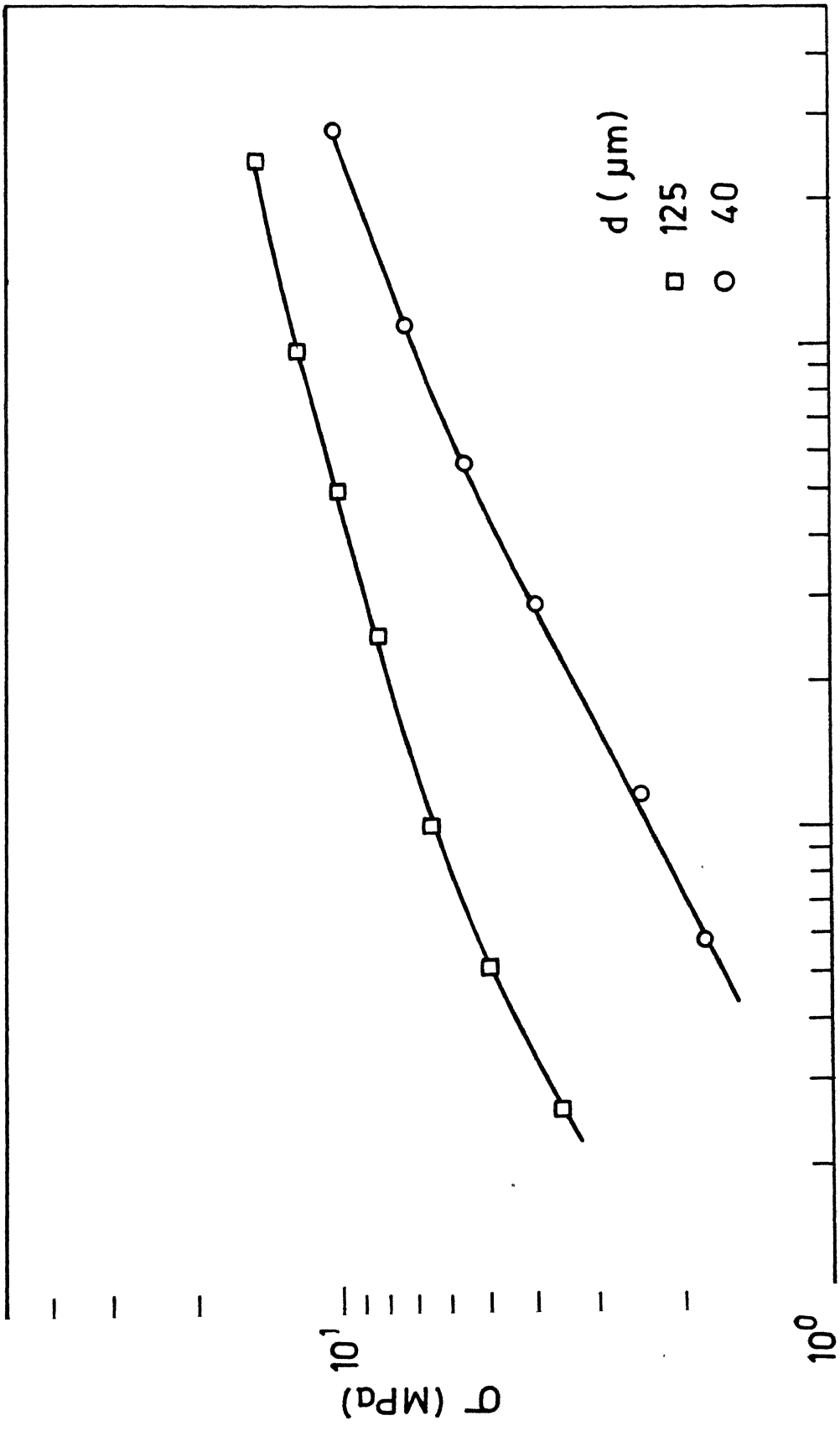

Fig. 7 Stress-strain rate plots for different grain sizes at 648K.

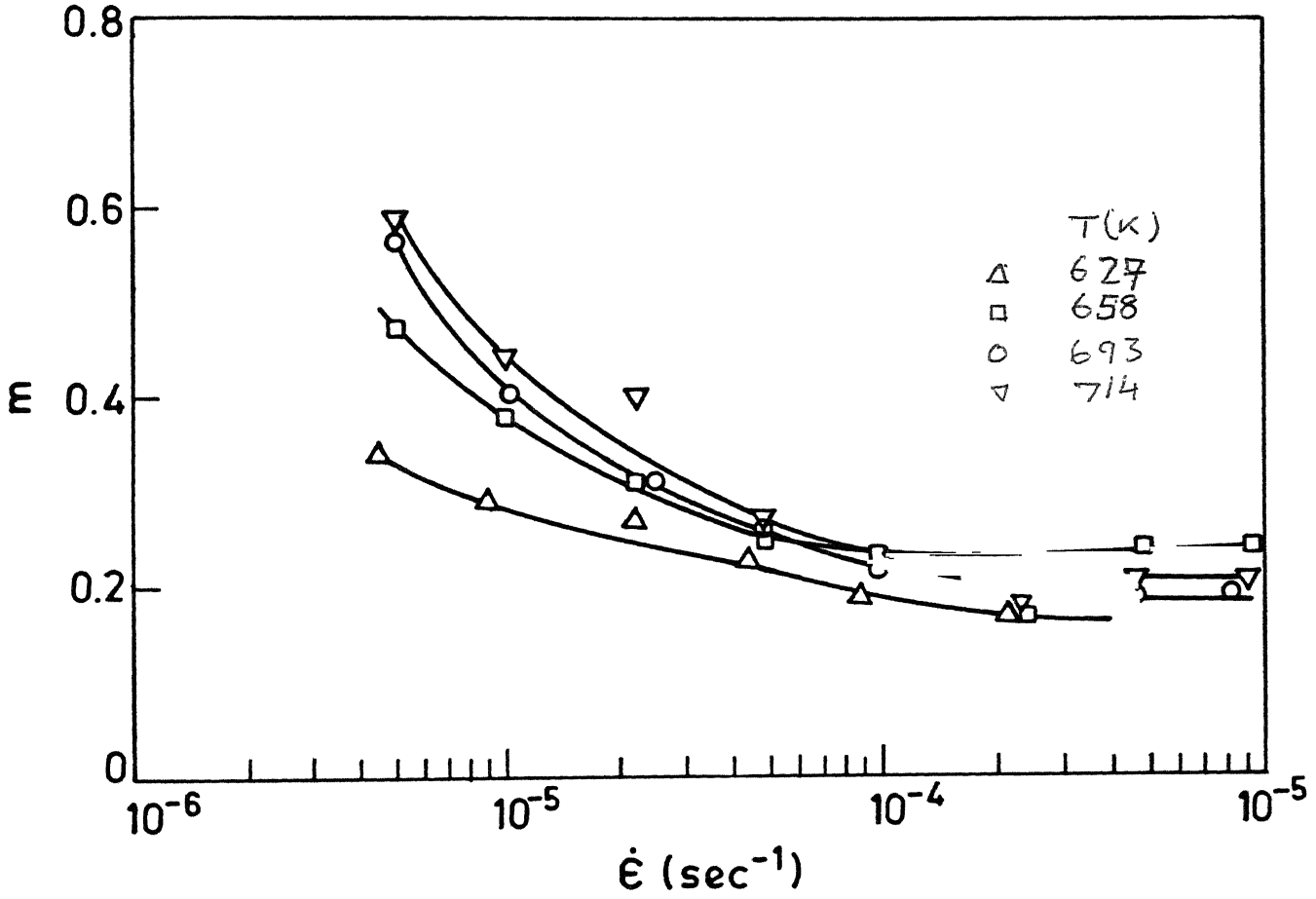

Fig. 8 Strain rate dependence of the strain rate sensitivity index at various temperatures (d = 125 μm)

The corresponding stress exponent (n) values are 2.0 and 5.0 in regions II and III respectively.

3.1.2(a) Grain Size Exponent

From equation (1), the grain size exponent 'p' can be written as

$$p = -\left[\frac{\log(\dot{\varepsilon}/\sigma^n)}{\log d}\right]_T \qquad (10)$$

Thus, at a given temperature, p can be determined by considering strain rate at a fixed stress level or stress at a fixed strain rate for various grain sizes. Alternatively, p can be estimated from the plot of $\log(\dot{\varepsilon}/\sigma^n)$ versus log d at constant temperature.

The grain size exponent was first estimated using constant strain rate and constant stress data in region II at temperature of 648 K. A strain rate of 5×10^{-6} sec^{-1} and a stress of 3 MPa were considered for this purpose. p at 648 K was also estimated from a plot of $\log(\dot{\varepsilon}/\sigma^n)$ versus log d (Figure 9). The value of the grain size exponent in region II is determined to be 1.9.

To determine the grain size exponent 'p' in region III it was noticed that steady state stress corresponding to this region was independent of grain size. This was confirmed from the strain rate cycling data (Figures 15 and 16). Since each cycle corresponds to a different initial grain size (as discussed latter) the grain size exponent 'p' in region III is zero.

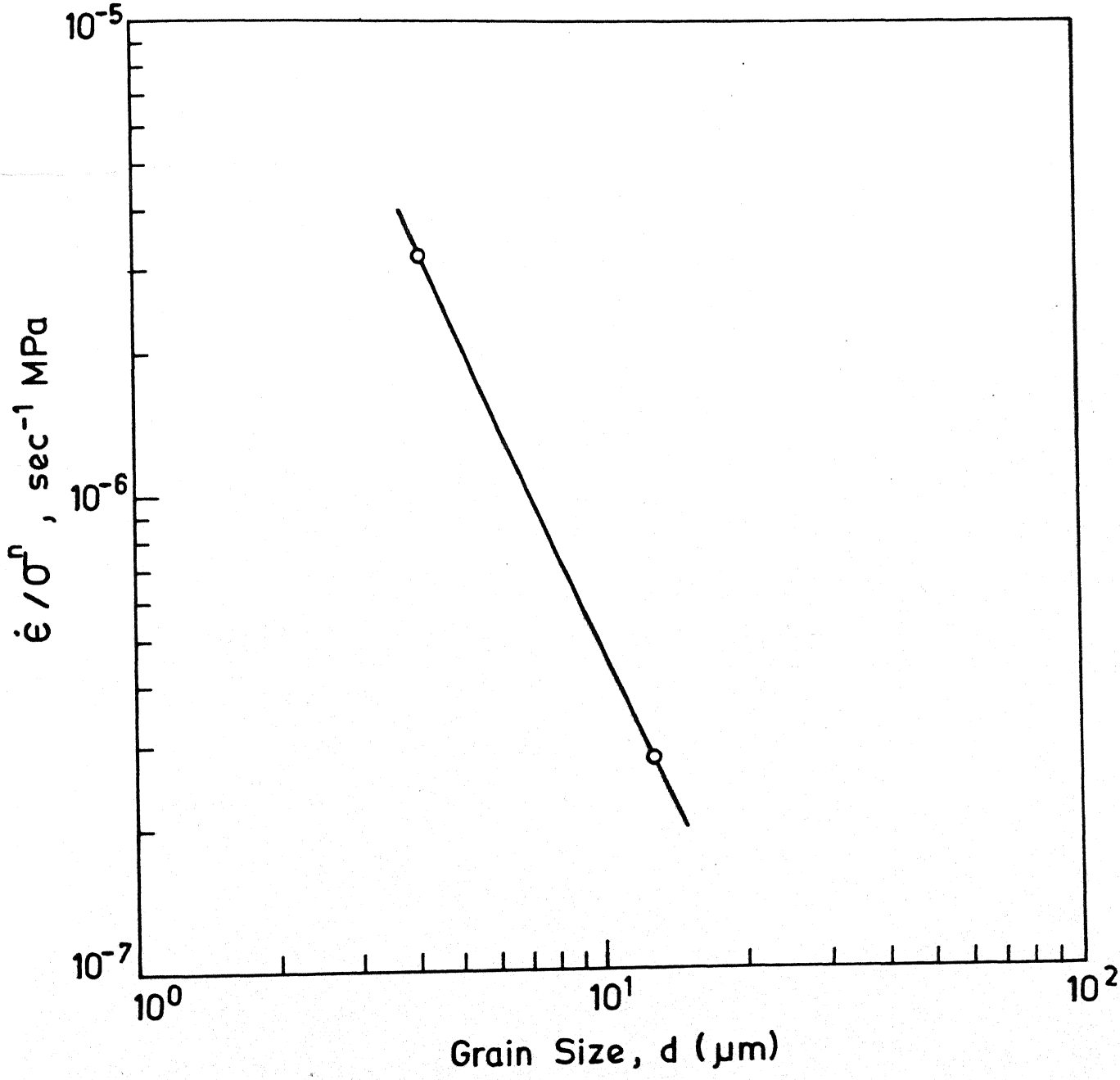

Fig. 9 Grain size exponent determination in region II at temperature of 648 K.

3.1.2(b) Activation Energy (Q)

It may be seen from the constitutive relation (1), that the activation energy can be evaluated by the equation:

$$Q = - R \left[\frac{\partial \ln(\dot{\varepsilon}\, T\, E^{n-1})}{\partial (1/T)}\right]_{d,\sigma} \qquad (11)$$

Activation energy values for deformation in regions II and III have been determined by considering the data for grain size at constant σ.

In region II, the activation energy value was determined by using the data corresponding to constant stress of 3 MPa for the grain size 125 μm. A typical plot of the logarithmic temperature compensated strain rate ($\dot{\varepsilon}\, T\, E^{n-1}$) versus the reciprocal of the absolute temperature at constant stress is shown in Figure 10. The observed activation energy value in this region is 67.3 KJ/mole.

In region III the value of activation energy was calculated using

$$Q = R \left[\frac{\partial \ln \dfrac{\sigma^n}{\dot{\varepsilon}\, T\, E^{n-1}}}{\partial (1/T)}\right]_d \qquad (12)$$

This plot for grain size is shown in Figure 11.

The observed Q value is 116.4 KJ/mole in this region.

3.1.2(c) Dimensionless Constant (A)

The constant A of the constitutive equation was determined from equation (1) by using the appropriate values of the parameters n, p and Q corresponding to regions II and

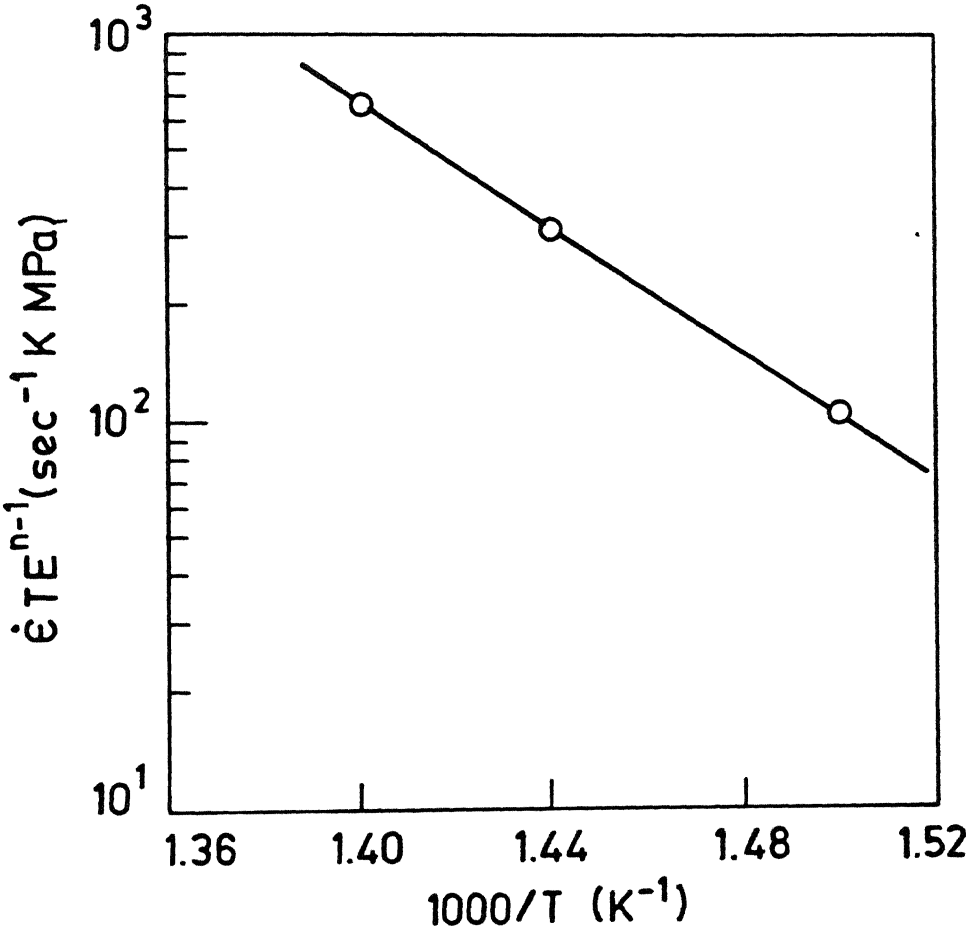

Fig. 10 Plot of temperature compensated $\dot{\epsilon}$ vs reciprocal temperature for grain size 125 μm.

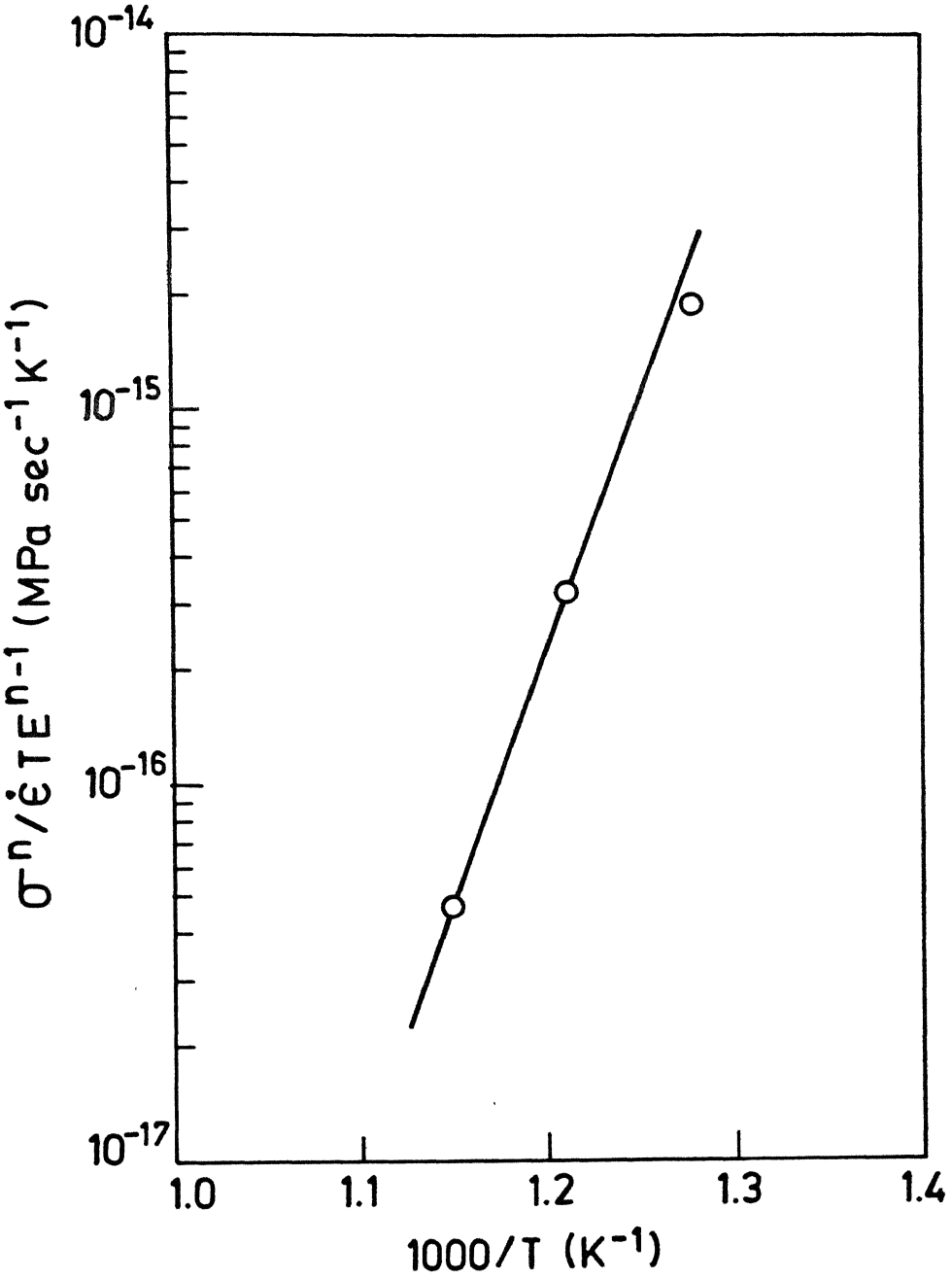

Fig. 11 Arrhenius plot for activation energy determination in region III .

III. Taking b value as 3.2 Å and D_o as 10^{-4} cm^2 sec^{-1} for both lattice and grain boundary self diffusion in magnesium the values of A are 2.6×10^6 and 2.2×10^{11} respectively.

Thus, the representative constitutive equations for regions II and III are summarized as follows:

(i) Region II

$$\dot{\varepsilon} = 2.6 \times 10^6 \frac{D_{o(gb)}\, E\, b}{kT} \left(\frac{b}{d}\right)^2 \left(\frac{\sigma}{E}\right)^2 \exp\left(-\frac{67.3}{RT}\right) \qquad (13)$$

(ii) Region II

$$\dot{\varepsilon} = 2.2 \times 10^{11} \frac{D_{o(l)}\, E\, b}{kT} \left(\frac{\sigma}{E}\right)^5 \exp\left(-\frac{116.4}{RT}\right) \qquad (14)$$

where, $D_{o(gb)}$ and $D_{o(l)}$ are pre-exponential factors in the grain boundary and lattice diffusion coefficients respectively and activation energy is given in KJ per mole.

3.2 Microstructural Instability

The stress-strain rate data for round specimens of grain size 40μm at very high temperatures, upto a maximum of 0.95 T_m, where T_m is the melting point of the alloy, are shown in Figure 12. Data could not be collected at strain rates lower than those indicated because of the weight of the lower pull rod of the test assembly which exceeded the flow stresses corresponding to those strain rates. Only region III can be observed at these high temperatures in the strain rate range investigated with the exception of data at 781 K where a transition state between regions II and III can be observed.

Comparison of these data with those shown in Figure 6 indicates that the transition strain rate between regions II and III at these very high temperatures is decreased which is in contradiction to the expected results. This suggests the presence of microstructural instability at these very high temperatures.

The strain effect on microstructure was studied through strain rate cycling. Figure 13 shows the $\sigma - \dot{\varepsilon}$ data obtained by two strain rate cycles for the round specimens of grain size 40 μm in a test at 623 K. It can be seen that the flow stresses in the second cycle are identical to those in the first cycle for the corresponding strain rates in both the regions II and III. Thus for these specimens strain did not influence the mechanical behaviour and hence the microstructure at this temperature.

However, the flat specimens show a different behaviour. Figure 14 shows $\sigma - \dot{\varepsilon}$ data for three strain rate cycles of the as received samples at a test temperature of 648 K. There was considerable increase in flow stress in region II at a given strain rate from first cycle to second beyond which the change was small. No change was observed in flow stress in region III as a result of repeated strain rate cycling. In another case $\sigma - \dot{\varepsilon}$ were collected for the flat specimens which were annealed at 673 K for 12 hrs (grain size 125 μm). Figure 15 shows the results obtained through repeated strain rate cycling upto the fourth cycle. Though there was some increase in flow stress at a given

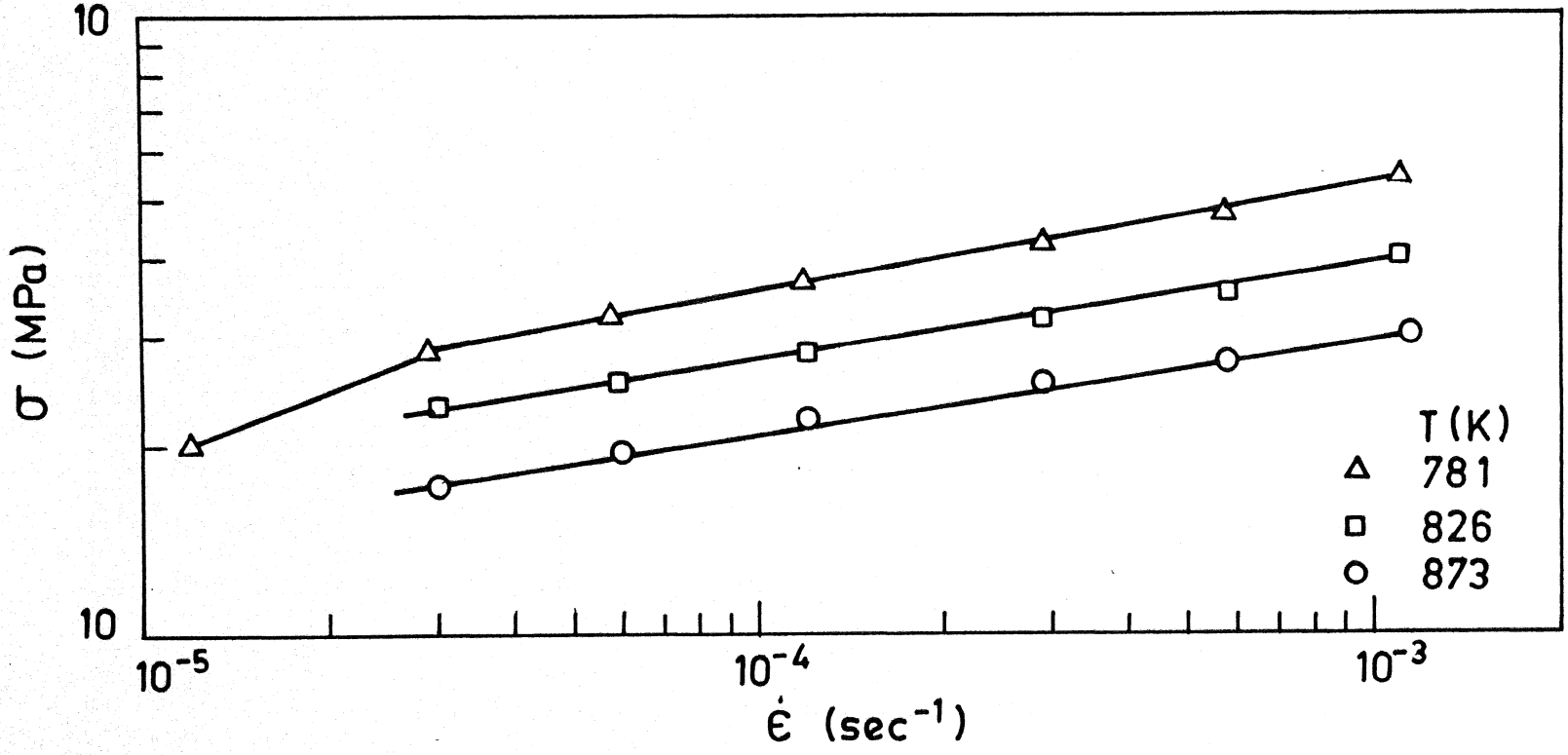

Fig. 12. Stress-strain rate plots at very high temperatures (d = 40 μm)

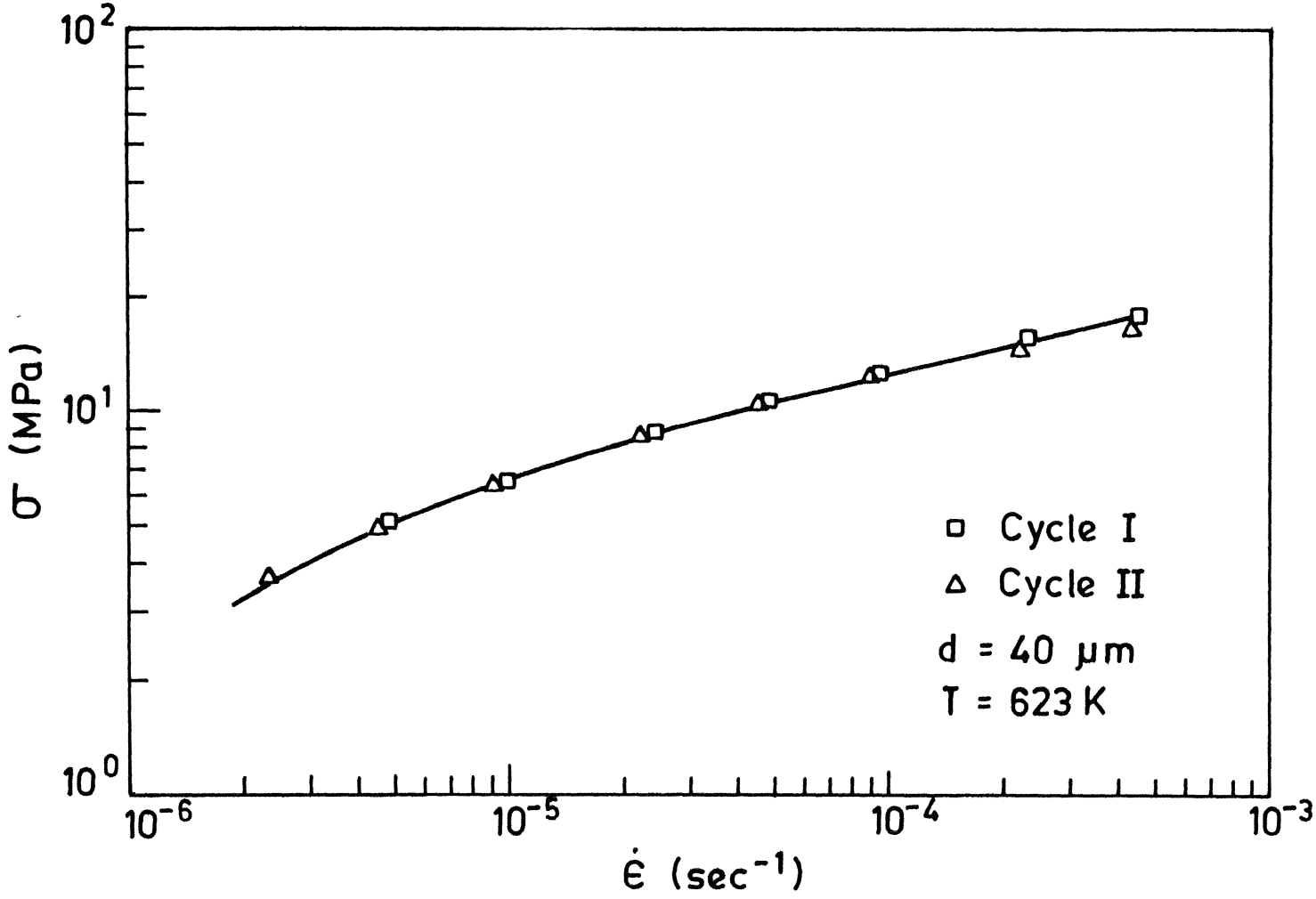

Fig. 13 Effect of repeated strain rate cycling on the $\sigma - \dot{\epsilon}$ behaviour.

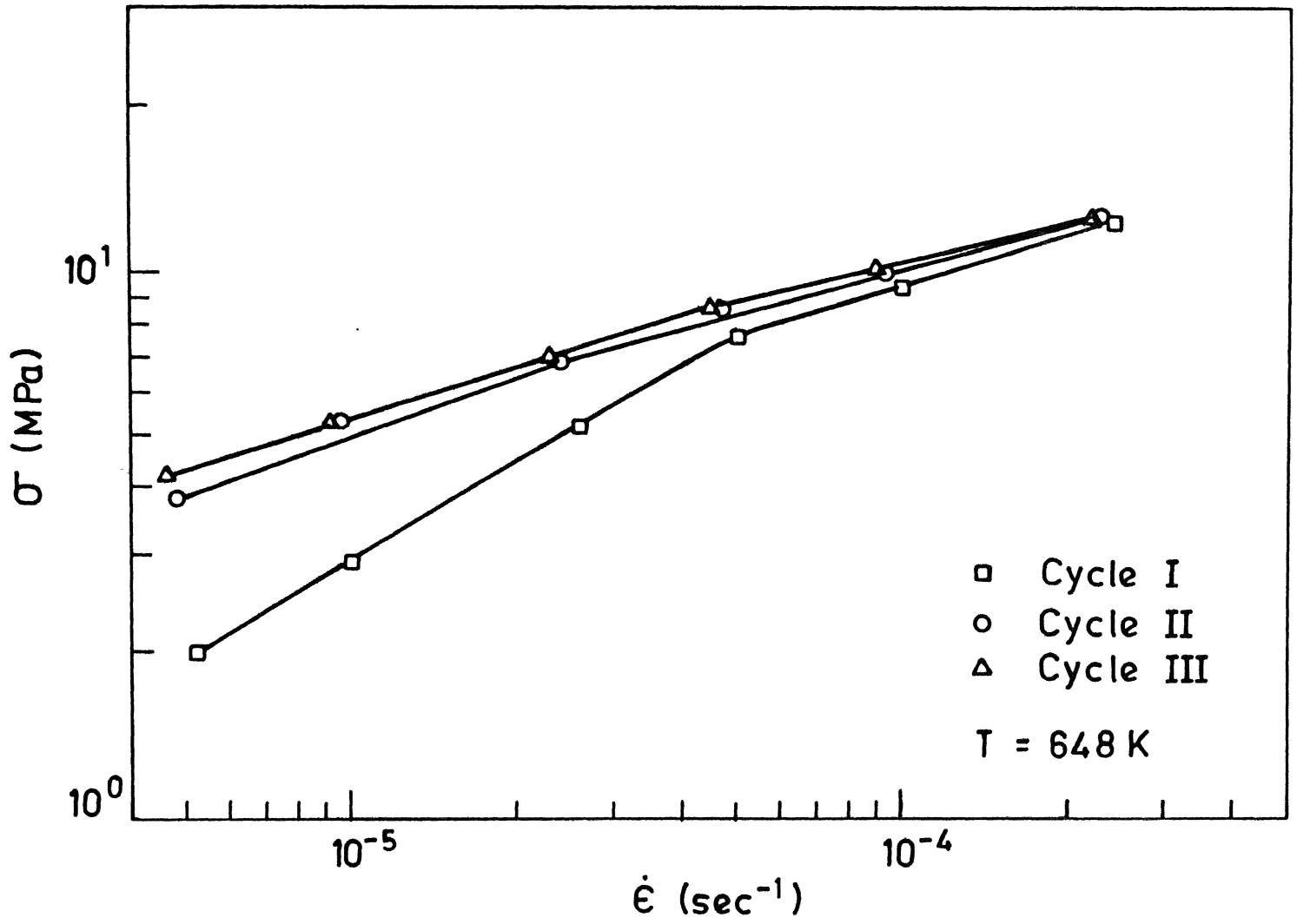

Fig. 14 Effect of repeated strain rate cycling on the σ - $\dot{\epsilon}$ behaviour of as received sheet specimens.

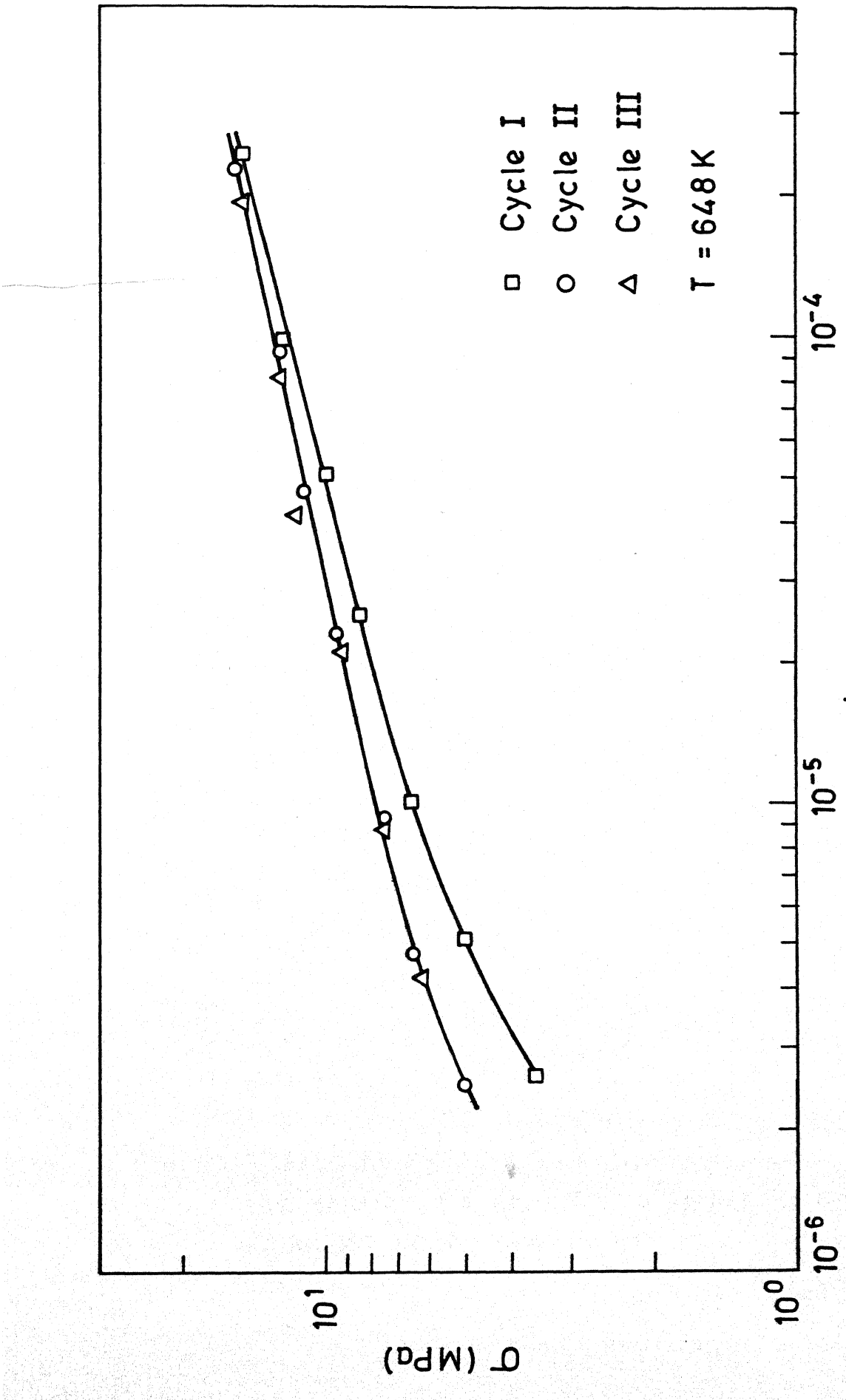

Fig. 15 Effect of repeated strain rate cycling on the σ-$\dot{\epsilon}$ behaviour of sheet specimens annealed at 673 K for 12 hours.

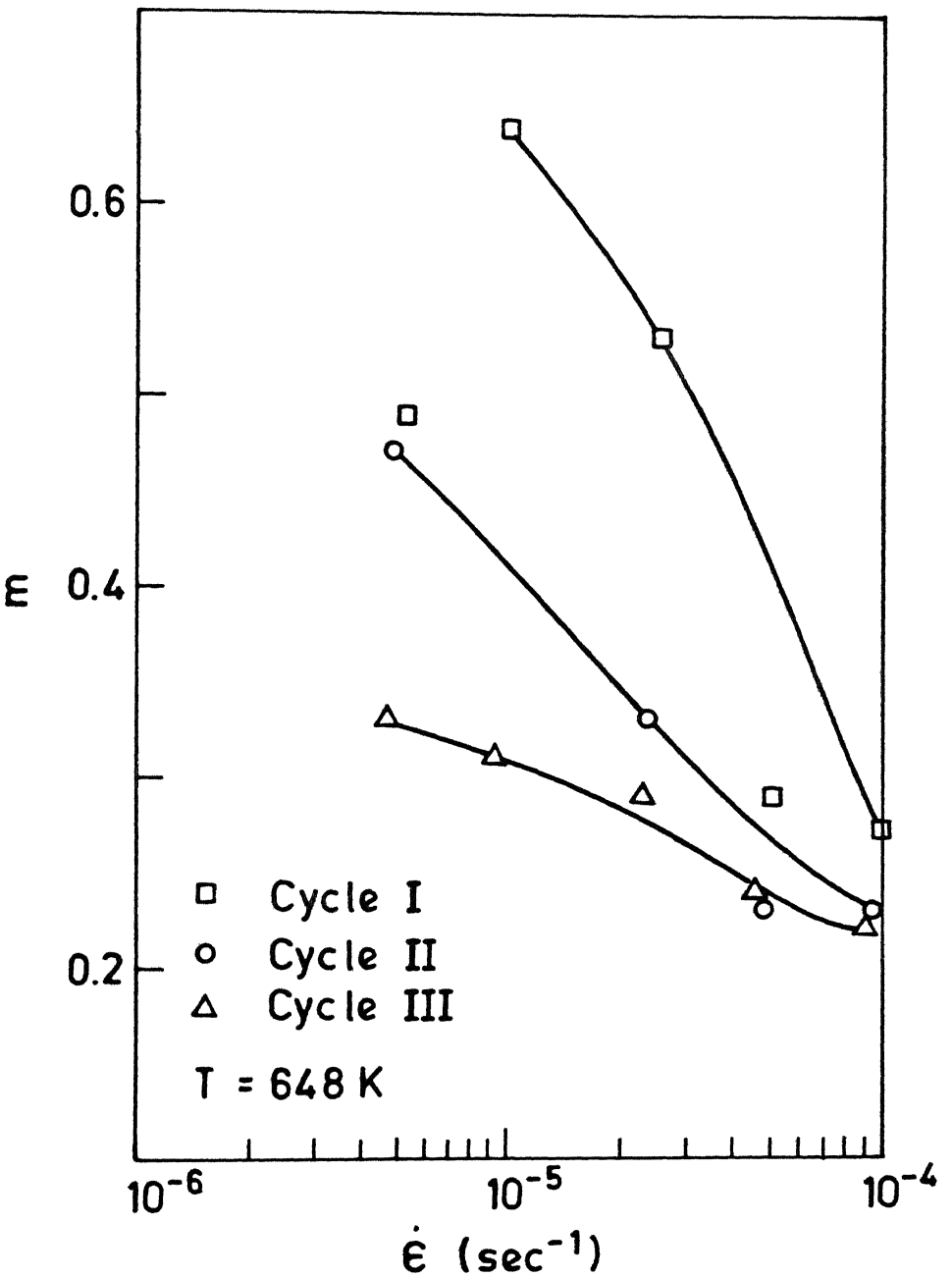

Fig. 16 Effect of repeated strain rate cycling on the strain rate sensitivity index of as received sheet specimen.

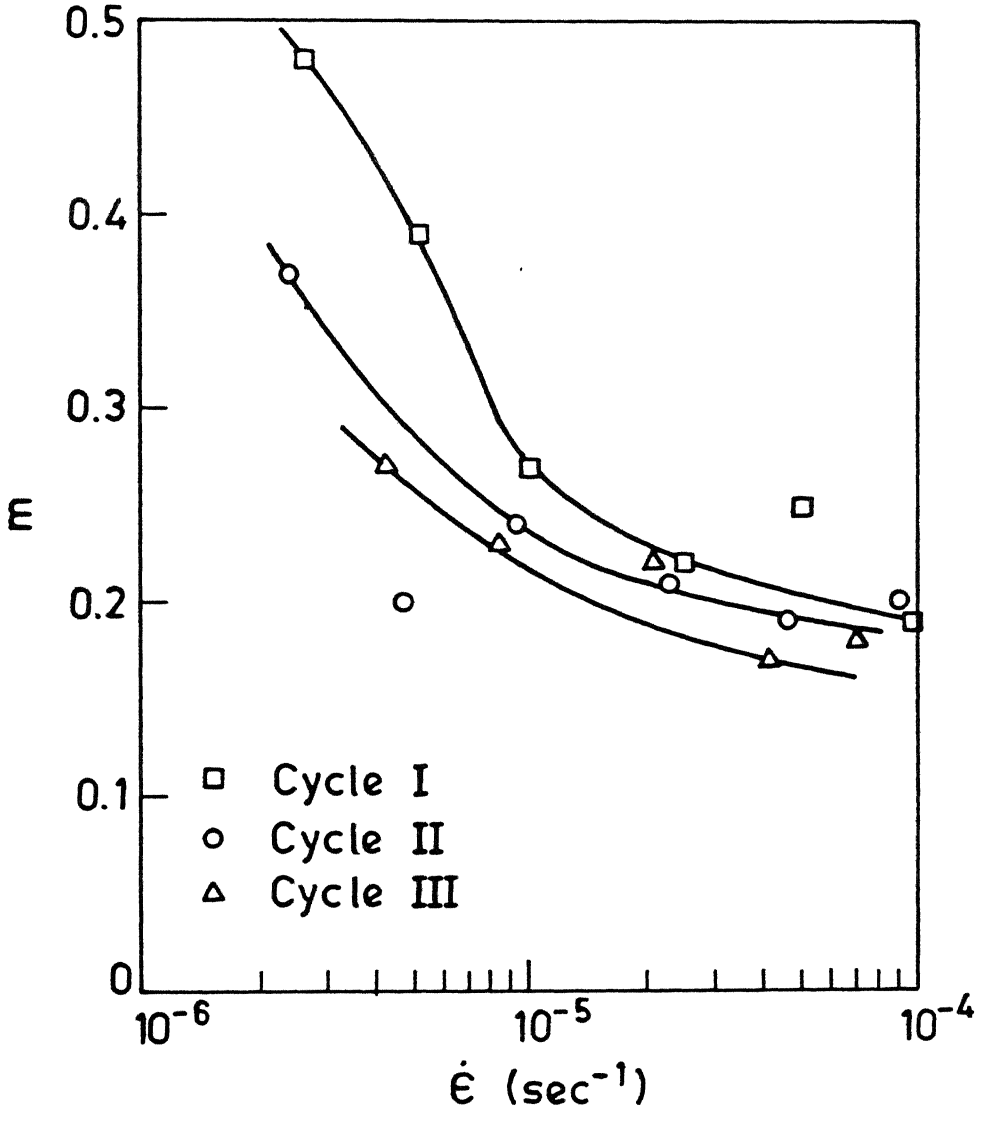

Fig. 17 Effect of repeated strain rate cycling on the strain rate sensivity index of annealed sheet specimens.

strain rate in region II form cycle I to cycle II no further change occurred in flow stress upto cycle IV. As in previous case flow stress was not affected in region III through these repeated strain rate cycling. Figures 17 and 18 show variation of strain rate sensitivity index 'm' with strain rate for as received and annealed flat specimens respectively at temperature 673 K. Though there was considerable decrease in m through repeated strain rate cycling for the as received flat specimen, the change was small for the annealed specimen.

3.3 Fracture Behaviour

3.3.1 Variation of Elongation with Strain Rate

Individual specimens of both the grain sizes were tested to failure at 648 K at different initial strain rates. Round specimens of grain size 40μm were tested at initial strain rates from 5.96×10^{-4} sec^{-1} in region III to 3.04×10^{-5} sec^{-1} in region II. And flat specimens of grain size 125 were tested to failure at initial strain rates from 2.89×10^{-4} sec^{-1} in region III to 1.49×10^{-5} sec^{-1} in region II. The stress-strain rate data for specimens of both the grain sizes at this temperature is shown in Figure 7.

Figures 18(a) and (b) show specimens of grain sizes 40μ and 125μ respectively after failure. In Figure 18(a) specimen A is untested and specimens B, C and D were tested at initial strain rates of 5.96×10^{-4} sec^{-1}, 1.2×10^{-4} sec^{-1} and 3.04×10^{-5} sec^{-1} respectively. In Figure 18(b) specimen A is untested and specimens B, C, D and E were

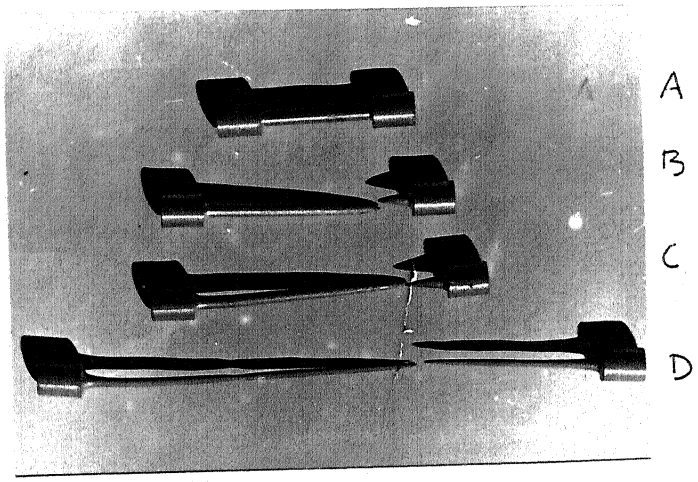

(a)

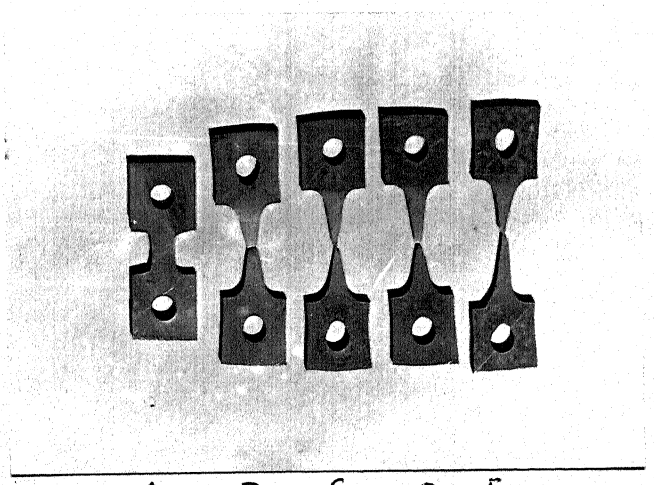

(b)

Fig. 18. (a) Specimens of Mg - 0.5% Zr alloy of grain size 40 μm pulled at 648 K; specimen A is untested and specimens B-D were pulled to failure at decreasing initial strain rates ranging from 5.96×10^{-4} sec^{-1} to 3.04×10^{-5} sec^{-1},
(b) Specimens of grain size 125 μm pulled at 648 K; specimen A is untested and specimens B-E were pulled to failure at decreasing initial strain rates ranging from 2.89×10^{-4} sec^{-1} to 1.49×10^{-5} sec^{-1}.

tested at initial strain rates of 2.89×10^{-4} sec^{-1}, 7.3×10^{-5} sec^{-1}, 2.87×10^{-5} sec^{-1} and 1.49×10^{-5} sec^{-1} respectively. The specimen D in Figure 18(a) shows evidence of diffuse necking whereas remaining specimens show evidence of localised necking and a consequent small increase in the area of the fracture tip at the lower elongations.

Figures 19 and 20 show the elongation to failure in tension $\Delta L/L_o$ against the initial strain rate $\dot{\epsilon}$, where ΔL is the increase in length at the point of fracture and L_o is the initial specimen gauge length. These figures also show m versus $\dot{\epsilon}$ plot. Elongation to failure increased with decrease in initial strain rate and increase in m for specimens of both the grain sizes. The maximum elongation to failure were 320% and 158% for specimens of grain sizes 40 μm and 125 μm respectively both occurring at the lowest strain rate investigated in region II. Figure 21 shows elongation to failure versus strain rate for both the grain sizes. Elongation to failure was more at a given strain rate for the specimens of smaller grain size of 40 μm.

3.3.2 Fracture Characteristics

Different specimens show different mode of fracture failure depending on the imposed strain rate. The specimen of grain size 40 μm which was tested at an initial strain rate of 3.04×10^{-5} sec^{-1} shows evidence of quasistable plastic failure. A close examination of this specimen (Figure 18(a)) shows that necking is diffuse rather than

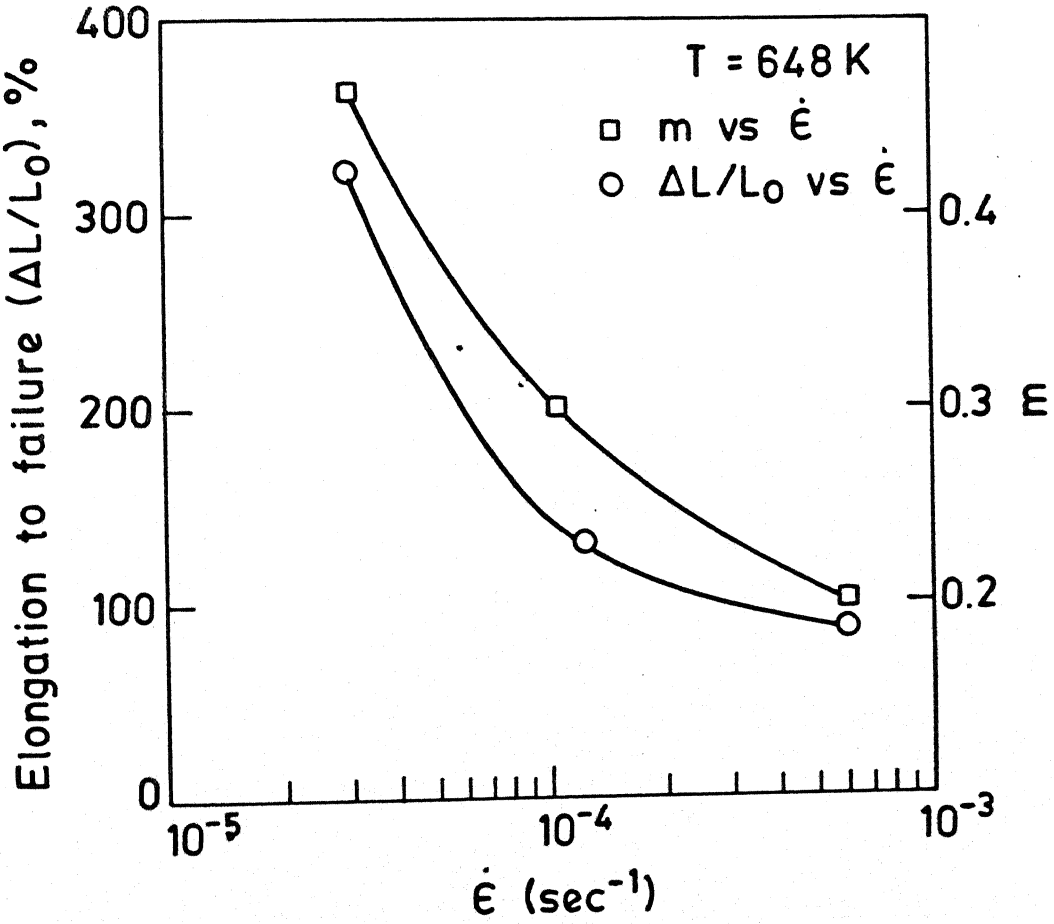

Fig. 19 Elongation to failure dependence on strain rate (d = 40 μm).

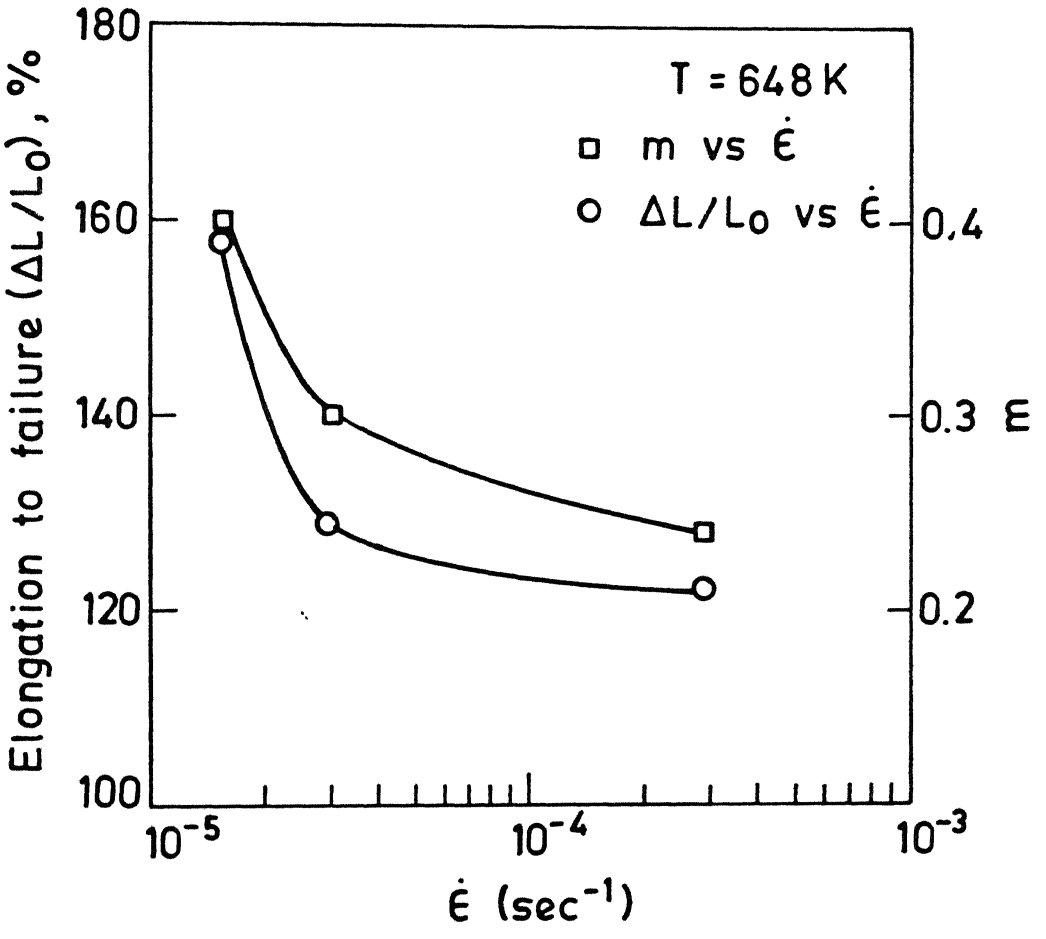

Fig. 20 Elongation to failure dependence on strain rate (d = 125 μm).

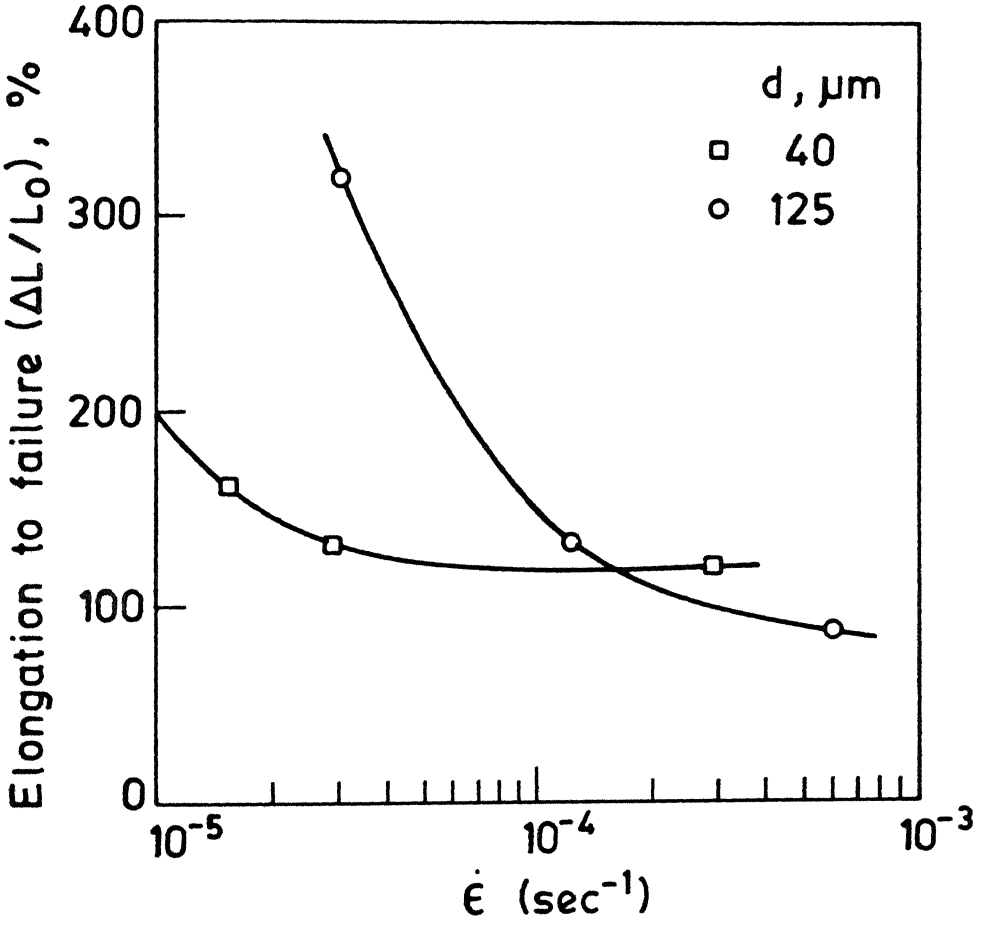

Fig. 21 Elongation to failure dependence on strain rate for both grain sizes at 648 K.

localized. However, this quasistable plastic flow ceased after few hundreds of per cent elongation and localized necking set in resulting in failure. Specimen C (Figure 18(a)) which was tested at an intermediate strain rate of 1.2×10^{-4} sec^{-1} failed by localized necking. And the mode of failure in specimen B tested at a large strain rate of 5.96×10^{-4} sec^{-1} is quasibrittle failure. This is evident from the low macroscopic elongation and a high value of A_f/A_i.

For specimens of grain size 125 μm (Figure 18(b)) failure occurred by localized necking in the initial strain rate range of 1.49×10^{-5} sec^{-1} to 7.3×10^{-5} sec^{-1} (specimens C, D and E). However, at a large initial strain rate of 2.89×10^{-4} sec^{-1} the specimen F failed by quasibrittle failure. These results are summarized in Table III.

Figure 22 shows the fracture surfaces of specimens of both the grain sizes. The surfaces show evidence of extensive cativation during deformation at all strain rates. However it is important to note that failure did not occur by 'cavitation'. There are fairly sharp ridges on all the fracture surfaces, and it is clear that final fracture occurred by a process of ductile rupture for all the specimens.

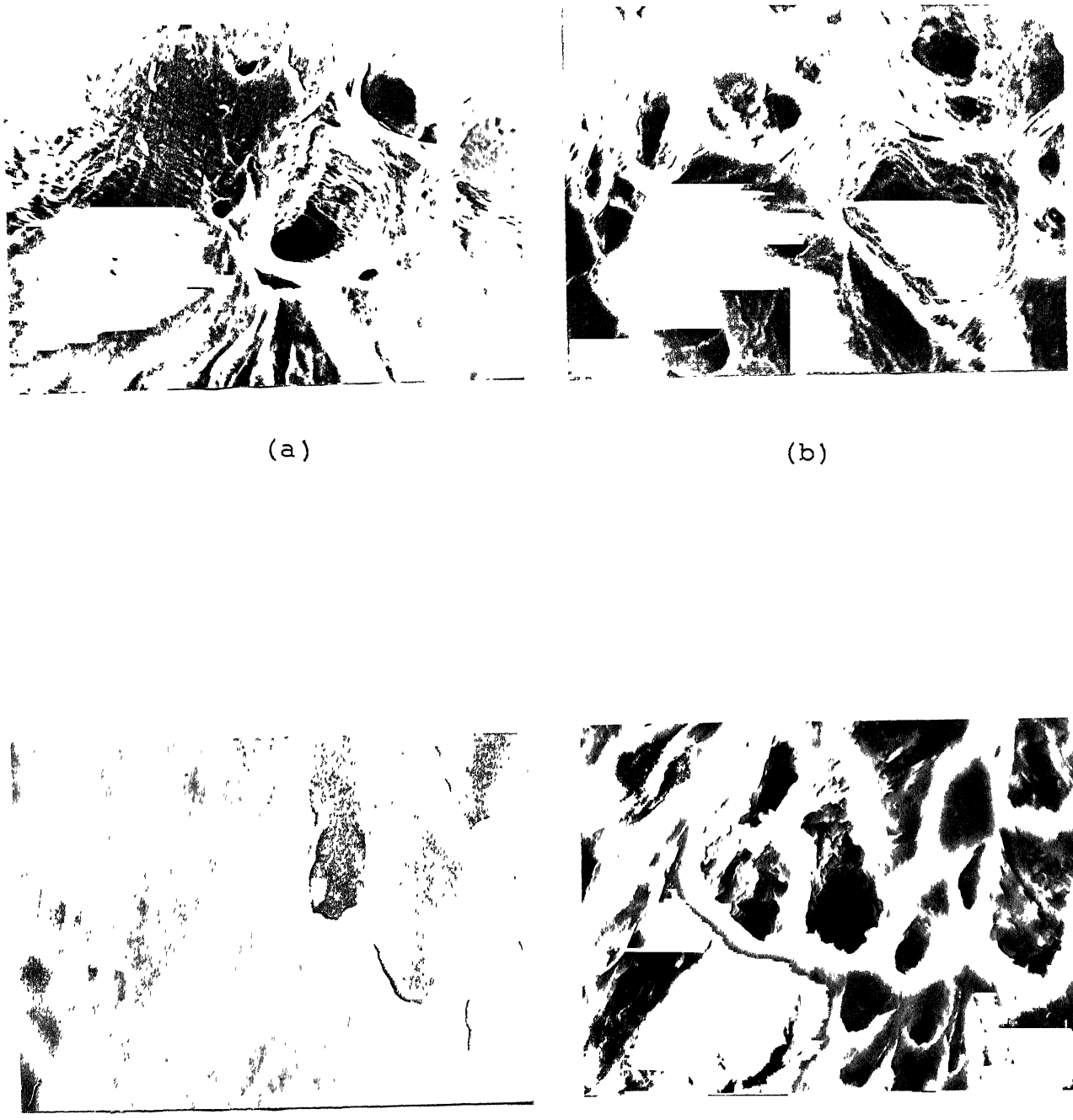

(a) (b)

(c) (d)

Fig. 22. Scanning electron micrographs of the fracture surfaces of specimens pulled to fracture at initial strain rates of (a) 5.96×10^{-4} sec^{-1} (d = 40 μm), (b) 3.04×10^{-5} sec^{-1} (d = 40 μm), (c) 1.49×10^{-5} sec^{-1} (d = 125 μm), (d) 2.89×10^{-4} sec^{-1} (d = 125 μm). Magnification: X400.

Table III

Observed types of failure

Grain size, μm	Initial strain rate, sec^{-1}	m	$\frac{\Delta L}{L_o}$, %	Fracture type
40	3.04×10^{-5}	0.46	320	Quasistable plastic flow → Necking
	1.2×10^{-4}	0.35	130	Necking
	5.96×10^{-4}	0.20	87	Quasibrittle
125	1.49×10^{-5}	0.25	158	Necking
	2.87×10^{-5}	0.22	129	Necking
	2.89×10^{-4}	0.17	120	Quasibrittle

CHAPTER IV

DISCUSSION

4.1 On the Mechanisms of Deformation in Regions II and III

In the investigated ranges of temperature, grain size and strain rate, only regions II and III are observed. It may be seen that the rate sensitive superplastic flow is observed even in specimens having a grain size of about 125 μm and thus superplastic flow is not restricted to grain sizes below 10 μm as commonly reported. In other words, the grain size effect is dominant in steady state deformation even at these very coarse grain sizes. To assess various deformation mechanisms that are operative in regions II and III the present results are compared with theoretical predictions. These comparisons are made below in the two regions separately for convenience.

4.1.1 Comparison of the Present Data with Theoretical Predictions in Region II

To assess the operative mechanisms in the superplastic region, the parameters of the constitutive equations n, P, Q and A determined from the experimental $\sigma - \dot{\varepsilon}$ data are compared with those predicted by theoretical considerations. This comparison based on the present experimental results and the values listed in Table II for different models are discussed below.

Among all the n values of the proposed mechanisms, the value of n = 2 in region II is closer to the present data. The models of Ball and Hutchison [20] and Mukherjee [21, 22] predict this kind of behaviour. The model proposed by Gittus [24, 25] also predicts similar value of n but it remains constant only at a stress level well above the threshold stress. All the other models excepting the N-H and Coble diffusional flow mechanisms predict a continuous change in n value with a limiting value of 1, which is inconsistent with the present $\sigma - \dot{\varepsilon}$ behaviour. The N-H and Coble mechanisms have the drawback of predicting a value of n = 1 in explaining the present data.

The grain size exponent prediction of 2 has been made in models except the Coble mechanism. The present value of P is closer to all these predictions.

In the case of activation energy for deformation, all mechanisms except the N-H diffusional flow predict a value which is equal to the grain boundary diffusion activation energy. Owing to the lack of a suitable tracer isotope no grain boundary self diffusion studies have been carried out on magnesium, so a direct comparison of the present value cannot be made. However, the observed value compares with the previous value of 80 KJ/mole calculated (from creep) by Jones [45].

The value of A is in disagreement with the predicted value of any of the mechanisms. However, the operative mechanism depends on the parameter A to a lesser extent only.

Thus the models by Ball and Hutchison [20], Mukherjee [21, 22] and Gittus [24, 25] are in better agreement with the present results, as far as the various parameters of the constitative relations are concerned.

4.1.2 Behaviour in Region III

The observed values of n and P are 5 and 0 respectively in this region. The observed value of activation energy compares with the previous value of the activation energy for lattice self diffusion (125 KJ/mole) calculated from creep by Vagarali and Langdon [46]. Typical parameters of dislocation climb controlled steady state creep are p = 0 and n = 4 - 5. The activation energy for deformation is equal to the lattice diffusion. Thus the present values are in good agreement with dislocation climb controlled recovery creep.

4.2 Microstructural Instability

About 30% strain is adequate to get a wide range of stress-strain rate data using differential strain rate test technique. This strain is considered to be low enough not to affect the microstructure, and therefore most of the experimental results on superplastic deformation are reported to be representative of steady state. In the differential strain rate test, the specimen is typically deformed to a small ($\sim$4%) strain at each individual strain rate. Hence one may not observe a distinct strain effect on flow stress at these individual strain rates. However, cumulative strain shows a

significant effect on flow stress due to microstructural instability. This suggests occurrence of a continuous change in microstructures and its gradual effect on flow behaviour during the span of deformation.

The occurrence of microstructural instability in the early part of deformation depends on the strain level, strain rate, test temperature, and the initial microstructural condition. The effect of test temperature can be seen by observing results in Figures 12 and 13. The repeated strain rate cycling at relatively low temperature of 623 K (Figure 13) indicates microstructural stability, because there is no increase in the flow stress at a given strain rate through repeated strain rate cycling. However, $\sigma - \dot{\varepsilon}$ data at very high temperatures (781 - 873 K) (Figure 12) show a decrease in transition strain rate between regions II and III. This is because of microstructural coarsening. Microstructural coarsening at these very high temperatures can be understood by considering the magnesium-zirconium binary phase diagram. The solid solubility limit of Zr in Mg is 0.1% at temperature below about 573 K. However, at 873 K this limits increases to 0.8% and the alloy containing 0.5% Zr is single phase at temperature greater than 798 K. Hence less precipitates are available at the grain boundaries at very high temperatures to prevent grain growth.

The specimens from the rolled sheet show mechanical instability and hence microstructural instability at test temperature close to 0.75 T_m. This instability is decreased

by annealing treatment of as received samples. This decrease in instability and hence evolution of microstructure towards more stable one is perhaps in the reduction of inhomogeneity in the as worked specimens on annealing treatment.

4.3 Fracture Behaviour

The value of strain rate sensitivity index 'm' governs tht role of necking through equation (3). Failure by necking becomes increasingly less important at higher values of m. This results in large elongation to failure at large values of m. The increase in elongation to failure with decrease in strain rate as shown in Figures 19 and 20 is because of increase in m with decrease in strain rate. And the higher value of elongation to failure for smaller grain size at a given strain rate (Figure 21) is due to higher value of m for smaller grain size.

The fracture characteristics depends on the imposed strain rate. At lower strain rate where the value of m is large, necking becomes diffuse rather than localised resulting in quasistable plastic flow. For the specimens of grain size 40 μm the value of m at the strain rate at which quasistable flow occurs is 0.46 which is quite large. However, this quasistable flow ceases after few hundreds of per cent elongation because of the growth of cavities. Formation of cavities decreases actual area of cross section and thus increasing effective stress resulting in localised necking. So the final fracture occurs by ductile tearing.

As the strain rate is increased i.e. m is decreased intrinsic plastic instability occurs in the material and failure occurs by necking.

Nucleation and growth of cavities are important factors in fracture failure by cavitation. However, though considerable formation of cavities occurs during deformation (Figure 18), in no case failure is by 'cavitation'. This is because ease of cavity formation and growth is not the only critical factor but ease of cavity interlinkage is also very important in governing final fracture. In the present study cavity interlinkage during deformation is found to be difficult.

CHAPTER V

CONCLUSIONS

1. In the investigated temperature and strain rate range regions II and III have been observed in the steady state deformation of Mg - 0.5% Zr alloy having grain sizes 40 μm and 125 μm.
2. The activation energy for deformation in region II is found to be 67.3 KJ/mole, which is close to that of grain boundary self diffusion in magnesium. The strain rate sensitivity index m is 0.5 ± 0.1 and it is relatively insensitive to temperature and grain size. The grain size exponent P is found to be close to 2.
3. The experimental results, on the basis of applied stress, are in better agreement with the analytical predictions of models of Ball and Hutchison, and Mukherjee that have been proposed for region II.
4. In region III the observed activation energy is 116.4 KJ/mole which is close to that of lattice self diffusion in magnesium. The strain rate sensitivity and grain size exponent are 0.20 ± 0.01 and zero respectively.

   In this region, the experimental observations are in good agreement with dislocation climb controlled creep.
5. Specimens from as received extruded rods do not show microstructural instability during deformation at

relatively lower temperatures. However, considerable coarsening occurs at temperatures close to melting point of the alloy. Specimens from as received rolled sheet show microstructural instability at intermediate temperatures and this instability is reduced by giving annealing treatment before testing.

6. Elongation to failure is observed to increase with decrease in strain rate and in turn with increase in strain rate sensitivity index, and also with decrease in grain size at a given strain rate.

7. Quasistable plastic flow is observed for specimens of grain size 40 μm at the lowest strain rate (region II) investigated. Necking and quasibrittle failures are observed at intermediate and high strain rates respectively.

8. Extensive cavitation occurs during deformation at all strain rates for both grain sizes. However, the final failure is not by 'cavitation'. This is because of the difficulty in interlinkage of cavities during deformation. Final failure occurs by ductile tearing.

REFERENCES

1. J.W. Edington, K.N. Melton and C.P. Culter, "Superplasticity", Prog. Mat. Sci., 21, 61 (1976).

2. A.K. Mukherjee, "Deformation Mechanism in Superplasticity", Ann. Rev. Mat. Sci., 9, 191 (1979).

3. D. Mclean, "Deformations at High Temperatures", Met. Rev., 7, 481 (1962).

4. J.E. Bird, A.K. Mukherjee, and J.E. Dorn, "Coarrelations Between High-Temperature Creep Behaviour and Structure", Quantitative Relation Between Properties and Microstructure, edited by D.G. Brandon and A. Rosen (Israel Univ. Press, Jerusalem), 255 (1965).

5. J. Weertman, "Dislocation Climb Theory of Steady State Creep", Trans. ASM, 61, 681 (1968).

6. A.K. Mukherjee, J.E. Bird and J.E. Dorn, "Experimental Correlations for High TemperatureCreep", Trans. ASM, 62, 155 (1969).

7. W.A. Backofen, I.R. Turner and D.H. Avery, "Superplasticity in an Al-Zn Alloy", Trans. ASM, 57, 980 (1964).

8. M.F. Ashby and R.A. Verrall, "Diffusion Accommodated Flow and Superplasticity", Acta Met., 21, 149 (1973).

9. M.L. Vaidya, K.L. Murty and J.E. Dorn, "High Temperature Deformation Mechanisms in Superplastic Zn - 22% Al Eutectoid", Acta Met., 21, 1615 (1973).

10. S.C. Misro and A.K. Mukherjee, "Rate Processes in Plastic Deformation", eds. J.C.M. Li and A.K. Mukherjee, ASME, Metals Park, Ohio, 434 (1975).

11. F.A. Mohamed and T.G. Langdon, "Creep at Low Stress Levels in Superplastic Zn - 22% Al Eutectoid", Acta Met., 23, 117 (1975).

12. F.A. Mohamed and T.G. Langdon, "Creep Behaviour in the Superplastic Pb - 62% Sn Eutectic", Phil. Mag., 32, 697 (1975).

13. H.W. Hayden and J.H. Brophy, "The Interrelation of Grain Size and Superplastic Deformation of Ni-Cr-Fe Alloys", Trans. ASM,61, 542 (1968).

14. T.G. Langdon, "The Mechanical Properties of Superplastic Materials", Met. Trans., 13A, 689 (1982).

15. R.C. Gifkins and T.G. Langdon, "Comments on Theories of Structural Superplasticity", Mater. Sci. Engg., 36, 27 (1978).

16. K.A. Padmanabhan and G.C. Davies, "Superplasticity", Springer-Verlag, Berlin and New York (1980).

17. T.G. Langdon, "Current Problems in Superplasticity", Creep and Fracture of Engineering Materials and Structures (eds. B. Wilshire and D.R.J. Owen), Pineridge Press, Swansea, Wales, 141 (1981).

18. R.C. Gifkins, "Mechanisms in Superplasticity", Superplastic Forming of Structural Alloys (eds. N.E. Paton and C.H. Hamiton, A Publication of the Metallurgical Society of AIME), 3 (1982).

19. A. Arieli and A.K. Mukherjee, "Superplasticity - Mechanical and Microstructural Affects", Preprint.

20. A. Ball and M.M. Hutchison, "Superplasticity in the Aluminium-Zinc Eutectoid", Metal. Sci. J., 3, 1 (1969).

21. A.K. Mukherjee, "High-Temperature Creep", Treatise on Materials Science and Technology, Vol. 6, Academic Press, New York, 164 (1975).

22. A.K. Mukherjee, "The Rate Controlling Mechanism in Superplasticity", Mater. Sci. Engg., 8, 83 (1971).

23. R.C. Gifkins, "Grain Boundary Sliding and Its Accommodation During Creep and Superplasticity", Met. Trans., 7A, 1225 (1976).

24. J.H. Gittus, "Theory of Superplastic Flow in Two-Phase Materials: Role of Interphase Boundary Dislocations, Ledges and Diffusion", Trans. ASME, 99, 244 (1977).

25. J.H. Gittus, "High Temperature Deformation of Two-Phase Structures", Phill. Trans. R. Soc. Lod., A288, 12 (1978).

26. K.A. Padmanabhan, "A Theory of Structural Superplasticity", Mater. Sci. Eng., 29, 1 (1977).

27. T.S. Ke, "A Grain Boundary Model and the Mechanism of Viscous Intercrystalline Slip", J. Appl. Phys., 20, 274 (1949).

28. J. Weertman, "Dislocation Climb Theory of Steady-State Creep", Trans. ASM, 61, 681 (1968).

29. C.R. Barrett, J.L. Lytton and O.D. Sherby, "Effect of Grain Size and Annealing Treatment on Steady-State Creep of Copper", Trans. Met. Soc. AIME, 239, 170 (1967).

30. R.C. Gifkins, "The Grain Size Dependence of Creep Rate in Recovery Creep", J. Aust. Inst. Metals, 18, 137 (1973).

31. A. Arieli and A. Rosen, "Measurements of the Strain Rate Sensitivity Coefficient in Superplastic Ti-6 Al-4 V Alloys", Scripta Met., 10, 471 (1976).

32. M. Shery and B. Baudelet, "Rheological and Metallurgical Discussion of Superplastic Behaviour", Rev. Phys. Appl., 13, 53 (1978).

33. S.W. Zehr and W.A. Backofen, "Superplasticity in Lead-Tin Alloys", Acta Met., 22, 1321 (1974).

34. H. Naziri and R. Pearce, "Superplasticity in a Zn - 0.4% Al Alloy", Acta Met., 22, 1321 (1974).

35. E.W. Hart, "The Tensile Test", Acta Met., 15, 351 (1967).

36. D.M.R. Taplin, G.L. Dunlop and T.G. Langdon, "Flow and Failure of Superplastic Materials", Ann. Rev. Mater. Sci., 9, 151 (1979).

37. D.A. Miller and T.G. Langdon, "Cavitation in a Superplastic Al-Zn-Mg Alloy", Trans. JIM, 21, 123 (1980).

38. T. Chandra, J.J. Jonas and D.M.R. Taplin, "Grain-boundary Sliding and Intergranular Cavitation During Superplastic Deformation of α/β Brass", J. Mater. Sci., 13, 2380 (1978).

39. C.W. Humphries, and N. Ridley, "Cavitation During the Superplastic Deformation of an α/β Brass", J. Mater. Sci., 13, 2477 (1978).

40. S. Sagat, P. Blenkinsop and D.M.R. Taplin, "A Metallographic Study of Superplasticity and Cavitation in Microduplex Cu - 40% Zn", 274 (1972).

41. M.J. Stowell, D.W. Livesey and N. Ridley, "Cavity Coalescence in Superplastic Deformation", Acta Metall., 32, 35 (1984).

42. N. Ridley, D.W. Livesey and A.K. Mukherjee, "Effect of Strain, Strain Rate and Temperature on Cavity Size Distribution in a Superplastic Copper-base Alloy", J. Mater. Sci., 19, 1321 (1984).

43. S. Shei, and T.G. Langdon, "The Fracture Characteristics of A Superplastic Single Phase Copper Alloy", J. Mater. Sci., 13, 1084 (1978).

44. T.G. Langdon, "Fracture Processes in Superplastic Flow", Metal. Sci., 16, 175 (1982).

45. R.B. Jones, Nature, 207, 70 (1965).

46. S.S. Vagarali and T.G. Langdon, "Deformation Mechanisms in H.C.P. Metals at Elevated Temperatures - I. Creep Behaviour of Magnesium", Acta Met., 22, 1969 (1981).

47. P. Griffiths and C. Hammond, Acta Met., 20, 935 (1972).

48. K.A. Padmanabhan, "Comments on Superplasticity in Large Grained Materials", Scri. Met., 7, 787 (1973).

.....	.....
.....	.....
.....	.....
.....	.....
.....	.....
.....	.....
.....	.....
.....	.....
.....	.....
.....	.....
.....	.....